Mohammad Mohaghar

DEVELOPING A NOVEL METHOD FOR PREDICTING NEARSHORE AND OFFSHORE WAVE ENERGY OF THE PORTUGUESE WESTERN COAST USING DELFT3D

Janeiro, 2014

UNIVERSIDADE DE COIMBRA

DEVELOPING A NOVEL METHOD FOR PREDICTING NEARSHORE AND OFFSHORE WAVE ENERGY OF THE PORTUGUESE WESTERN COAST USING DELFT3D

Dissertation for Master of Science in Energy for Sustainability

Author: Mohammad Mohaghar
Student Number: 2012100628

Supervisor: Prof. Almerindo Domingues Ferreira

Acknowledgements

Abstract

This thesis is an investigation of wave power resources in the Portuguese western coast, focusing on the spatial distribution of wave power of coastal region exposed to the highest wave power. The main objective of the study is to provide a detailed description of the spatial distribution of wave power to assist the selection of locations for deployment of Wave Energy Converter (WEC) units in these zones. The study methodology employed to achieve this main objective entails an analysis of modeled wave data at nine wave stations distributed along the Portuguese western coast. The analysis provided a general description of wave power at locations for which wave data is calculated. From this analysis the location exposed to the highest wave power and the one with the most frequent waves were discovered.

The study objective was achieved by the Simulating Waves Nearshore (SWAN) model embedded in Delft3D software package with the help of Delft-Dashboard software. The ocean wave data were obtained for a 25-day computational period. A simplified simulation procedure was required in order to make the study practically feasible. The accuracy of the modeled output was investigated by directly comparing it to wave data recorded during the overlapping recording period. It was found that the model slightly underestimated the wave power compared to the measured data with a maximum underestimation of 11%; which is sufficiently accurate for the purpose of this study.

The results of this investigation alongside the new method discussed in this thesis can be used for the identification of areas with high wave power concentration in order to find the most suitable location to install the WEC units. Further numerical modeling is required for the detailed design of wave farms, especially if potential sites are located in shallow water.

Keywords: Wave energy, Delft3D, SWAN, Bathymetry, Nearshore, Offshore

Table of Contents

List of Symbols

L	Wavelength	m
T	Wave period	S^{-1}
h	Water depth	m
H	Wave height	m
$E(\sigma, \theta)$	Wave energy spectrum	
J	Wave power level	W/m
ρ	Sea water density	Kg/m^3
C_g	Group velocity	m/s
g	Gravitational acceleration	m/s^2
θ	Wave direction	Degrees
σ	Relative frequency	Hz
H_s	Significant wave height	m
$E(\omega, \theta)$	Variance density spectrum	
ω	Absolute radian frequency	Hz
N	Action density	
c_x	Propagation velocity in x-space	m/s
c_y	Propagation velocity in y-space	m/s
c_σ	Propagation velocity in σ-space	m/s
c_θ	Propagation velocity in θ-space	m/s
F_{xy}	Radiation stress induced force	N/m^2
τ_b	Bed shear stress	N/m^2
u_*	Friction velocity	m/s
v_t	Horizontal eddy viscosity	m^2/s
D	Dissipation of wave energy	N/ms
D_p	Peak wave direction	Degrees
γ	Peak enhancement factor	
h_{msi}	Measured significant wave height	m
h_{mdi}	Modeled significant wave height	m
$\overline{h_{ms}}$	Mean value of measured wave height	m
$\overline{h_{md}}$	Mean value of modeled wave height	m

List of Figures

List of Tables

1. Introduction

1.1. Problem statement

Today, most countries around the world have been feasting heavily on fossil fuels to generate and produce their electricity, and this has been jeopardizing the stability of the Earth's climate, threatening the health of its citizens and depleting the world of its natural resources leaving very little or nothing for the future generations. These concerns have necessitated an urgent search for alternative sources of energy. One of the most powerful forms of renewable energy is ocean energy, including wave and tidal. This type of energy can produce a significant amount of electricity without resorting to coal or gas-fuelled generators with limited environmental impacts [1].

There is a wide variety of wave energy technologies and wave energy convertors, depending on their water depth and location (i.e. shoreline, nearshore and offshore). Several methods have been proposed to classify wave energy systems according to location, working principle and size. Figure 1 demonstrates an example of such classification based on the "working principle" [2].

Oscillating water column (with air turbine)
- Fixed structure
  - Isolated: _Pico, LIMPET
  - In breakwater: Sakata, Mutriku
- Floating: Mighty Whale, Ocean Energy, Sperboy, Oceanlinx

Oscillating bodies (with hydraulic motor, hydraulic turbine, linear electrical generator)
- Floating
  - Essentially translation (heave): AquaBuoy, IPS Buoy, FO3, Wavebob, PowerBuoy
  - Essentially rotation: Pelamis, PS Frog, SEAREV
- Submerged
  - Essentially translation (heave): AWS
  - Rotation (bottom-hinged): WaveRoller, Oyster

Overtopping (with low-head hydraulic turbine)
- Fixed structure
  - Shoreline (with concentration): TAPCHAN
  - In breakwater (without concentration): SSG
- Floating structure (with concentration): Wave Dragon

Figure 1. The various wave energy technologies [2]

In this work, a novel method is introduced and developed in order to calculate wave energy in nearshore and offshore areas and to help predict wave behavior as accurately as possible. Delft3D is used to simulate nearshore and offshore (i.e. zones with deeper depth and farther distance from coastal lines) waves by taking flow hydrodynamics into account. The software uses a third generation wave model, namely SWAN in order to simulate wave parameters. Such energy prediction and calculation methods can be applied to different types of oscillating bodies. These oscillating bodies are basically offshore devices (sometimes classified as third generation devices) which are either floating or (seldom) fully submerged. They exploit the more powerful wave regimes available in deep water (typically more than 40 m). Offshore wave energy converters are in general more complex compared with first generation systems (e.g. oscillating water columns) [3,4].

1.2. Motivation

The harnessing of energy is one of the most critical challenges at the forefront of all of humanity's concerns. It affects societies in almost all aspects, including economic, social, political, military, and technological venues. In recent years renewable energy has become a pressing matter for the latest generation of engineers and researchers. They are confronted with the responsibility of designing environmentally safe products which require less conventional energy that run on cleaner renewable fuel. This project is a commitment to further realize these efforts by predicting new methods for calculating wave energy. Nowadays, predicting and calculating wave energy is one of the most important and complicated problems for engineers, because they need to find the most suitable areas where waves have the highest potential for energy extraction.

Among other alternatives, there have been advancements promoting the use of solar, geothermal, bio-fuel, and wind energy. But in order to keep up with the demands of today, more progress is needed. Fossil fuels will not last indefinitely and it quickly becomes imperative that alternatives be developed to the point that they become viable and readily available for all people and societies to use. I consider harnessing and using ocean wave energy which can potentially, in the long run, alleviate the current dependence on conventional fuel.

1.3. Aim of the study

The main purpose of this study is to predict, evaluate and compare the wave energy potential between different locations of Portuguese western coast, by using the available wind and wave boundary data. Nine different coastal regions are selected. This study uses the Delft3D and Delft-Dashboard software. All parameters for swell and wind wave data are extracted from online database for any given coastal and offshore location.

The results are provided separately for selected locations and entirely for the region in scope. The term wind wave refers to ocean waves caused by winds over ocean surface. Nevertheless, in this study the term "Wind Wave" is used for wind-generated waves, encountered in their generation zone.

Verification of Delft3D, and its reliability, for application in case of nearshore and offshore, is an essential subject for study to be addressed in this research. The SWAN coastal wave model is used for calculating wave energy in this study.

1.4. Thesis overview

The literature review of Chapter 2 comprises a brief explanation of wave power in Portugal. Consequently, the relevant wave theory and wave power related parameters are presented in a wave power calculation procedure. The literature study is concluded with a discussion of the current wave energy conversion technologies which can be used for the results section of this thesis. Furthermore, Delft3D flow and wave module, SWAN wave model and Delft-Dashboard software work principles are explained in this chapter.

Verification of the method which I have proposed is investigated in Chapter 3. The result of the wave power analysis of measured wave data recorded at wave recording stations along the Matosinhos coast is presented in this chapter, and then, they are compared with software results in order to verify the method. The accuracy of the model output is investigated by comparing software results with the online measured wave data. Also, the effect and the importance of time-varying boundary conditions are investigated on the results and similarity of the modeled and measured data.

The input data which is used in the SWAN and Delft3D software and the assumptions in some input data are explained thoroughly in the Chapter 4.

In Chapter 5, the statistical output from the wave power analysis will provide a general description of the wave power distribution along the Portuguese coastline. This chapter is concluded with the identification of the coastal zone with the greatest wave power resource. Also, the offshore wave data is initially analyzed and compared to the wave data recorded at shallower water locations.

Chapter 6 presents the conclusions drawn from this wave power resources investigation and the new method which is discussed in the thesis, and finally, recommendations for future works are presented in Chapter 7.

2. Literature Review

2.1. Wave energy potential in Portugal

Approximately 70% of the Earth is covered with water which consequently makes wave energy highly abundant. The amount of energy that can be extracted from waves varies depending on location, time of the year, month, day, etc., and also on weather conditions. Nevertheless, wave energy can be accurately predicted within a time period of a few days using numerical models.

Recent publications have shown that the ocean waves with the highest amount of energy mainly exist along the western edge of the Earth's continents in the $40\,° - 60\,°$ latitude range north and south due to the prevailing west-to-east winds. The annual average power for the waves varies in this part of the world between 30 and 70 kW/m, with peaks reaching up to about 100 kW/m in the Atlantic southwest of Ireland, in the Southern Ocean and near Cape Horn [5]. Australia, New Zealand, UK, Portugal, and Norway also have substantial wave power potential. That is due to the fact that they are all located at relatively high latitude and have a long stretch of ocean immediately to the west. *Clément* et al. [6] has given a detailed description of the status and perspective of wave energy in Europe.

Throughout the years, Portugal has proven to be a very popular location among those seeking to develop wave energy and also a number of companies have considered testing their prototype devices there. The potential for the wave energy extraction in the Portuguese coast can be obtained from analysis of the wave climate, where buoy data can give a general idea of the existing conditions.

To find out how much energy can be extracted from a potential source of wave, one needs to accurately analyze the wave climate. Similar to any other form of analysis and simulation, there is preliminary a need for initial conditions such as buoy data which are readily available online for certain periods of time and that can give a good idea of certain valuable information. Nevertheless, this approach faces its own limitations since the time period of the measurement is generally limited and buoys are usually operating in deep water.

Hence, it is highly important to develop a system that is able to predict the wave characteristics in different coastal locations which are not necessarily all considered as deep water. That is why it is essential to predict the wave conditions with numerical models.

An earlier attempt to develop a nearshore wave atlas for Portugal has been reported by Aguiar et al. [7]. Their work was based on the wind fields from an 11-year hindcast made with a model similar to a WAM-model – which is a wave generation model that gives appropriate results for the processes of wave generation and deep water propagation – where they coupled a wave model with an inverse ray refraction model which transforms directional spectra from deep water to nearshore in order to obtain results for coastal areas.

One of the most thorough and highly-developed hindcast studies which has been ongoing for almost 44 years is the Hindcast of Dynamic Processes of the Ocean and Coastal Areas of Europe (HIPOCAS) project which includes the Portuguese coast, as well as the whole European coast [8,9], providing a database four times as large as the one mentioned above. Their study used WAM, and so, it is applicable mainly for deep water [10].

That model was extended so as to make wave predictions for the finite water depth coastal environment using the SWAN model that was designed especially to account for the more complex physical processes that take place in intermediate and shallow water [11]. This represents a higher quality prediction than the one using a ray model [7].

The present work aims to demonstrate the effectiveness of using such a complex wave prediction system, based on Delft3d flow and wave models, for assessing the spatial distribution patterns of the wave energy in the Portuguese nearshore and offshore coasts.

2.2. Wave energy converters (WECs)

This section introduces WECs in terms of their classifications according to their distance from the shoreline and the types that can be implemented in both nearshore and offshore areas according to the results of this thesis.

2.2.1. Classification according to distance from the shoreline

One of the ways to classify WECs is according to their distance from the shoreline, and these types of devices are hence called shoreline, nearshore and offshore WECs. Shoreline WECs are embedded in the shoreline, which makes them easier to install and maintain. Also, unlike

some other technologies, shoreline devices do not require long lengths of underwater electrical cable. However, they have their disadvantages too such as the fact they usually experience a much less powerful wave regime and also their installation faces some limitations due to the requirements for shoreline geology, tidal range, preservation of coastal scenery etc. The most advanced group of shoreline devices is the oscillating water column. Versions of these devices include the Limpet, the European Pilot Plant on the island of Pico in the Azores and the Wavegen.

The second type of this category, namely nearshore WECs are set up at moderate water depths around 20-30 m, at a distance of up to around 500 m from the shore. They basically have the same advantages as shoreline devices, being at the same time exposed to higher wave power levels.

The last one in the group is the offshore WECs, which undergo more powerful wave regimes available in deep water with water depths over 40 m. These devices are located at or near the surface (i.e. floating) to help extract the maximum amount of energy from the waves, and so they usually require flexible electrical transmission cables. Before, overseas designs used to harness ocean wave energy were relatively small, modular devices, yielding high power output when arranged in arrays. In comparison to the previous multi-megawatt designs, these small size devices were rated at a few tens of kilowatts each. They have still proved to be popular and so, recent designs for offshore devices have also concentrated on small, modular devices.

2.2.2. Suitable Wave Energy Converters (WECs) for this method

This section briefly explains about the types of WECs that can be used for nearshore and offshore areas where the results of simulation are later obtained.

2.2.2.1. Attenuator

WECs which are aligned parallel to the actual direction of wave propagation (so that they effectively ride the waves) are called attenuators [12, 13]. When the attenuator is riding the waves, the constant changing of wave heights along the length of the device causes inward and outward stretching where the segments connect. This so-called flexing produces forces and moments which are captured as a form of hydraulic pressure, which in turn produces

energy. An advantage of the attenuator is that it has less of an area perpendicular to the waves, and so it experiences smaller forces [14].

One of the most well-known attenuators is the Pelamis. The Pelamis is a long and narrow (snake-like) semi-submerged structure which points into the waves as shown in Figure 2. It is composed of long cylindrical pontoons connected by three hinged joints. In order to produce electricity, this device firstly uses relative yaw and pitch motions between sections to capture wave energy [15] by pressurizing a hydraulic piston arrangement and then turns into a hydraulic turbine [16, 17]. Other examples of WECs which are classified as attenuators can also be found in the literature, such as the McCabe wave pump, the Ocean Wave Treader and the Wave Treader [18] and the Waveberg [19].
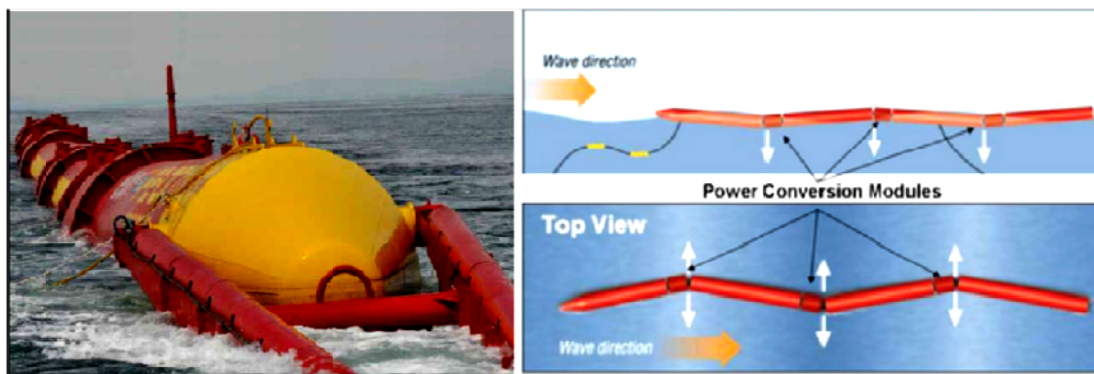
Figure 2. The Pelamis Attenuator[1]

The Pelamis power take off (PTO) has a set of hydraulic cylinders that pump fluid, via control manifolds, into high-pressure accumulators for short-term energy storage. Hydraulic motors use the supply of high-pressure fluid from the accumulators to drive grid-tie electric generators.

The Pelamis PTO can be examined and developed in two separate parts, which can be called the primary and secondary transmission. The primary transmission is in charge of converting the work done by the waves on the structure into stored energy. The secondary transmission, then converts the energy stored in the hydraulic accumulators into electricity which is eventually transmitted to the shore.

The moment produced by the impeding joints provided by the cylinders must change throughout each wave cycle such that the waves do the maximum work on the machine as a

---

[1] Images obtained online from http://www.eoearth.org/view/article/157027/

whole. In order to control the joint moment, one needs to use sets of electronically controlled valves, which control the flow of fluid between the hydraulic cylinders and the accumulator and reservoir. The valves are controlled to enable different combinations of chambers to contribute to the applied joint moment.

The only inefficiencies in the Pelamis PTO are associated with the losses due to the compressibility, bearing and seal friction of the hydraulic cylinders, and flow losses through valves and pipes. Such combined losses can be reduced to well under 20% by careful and well thought-out designs over a wide range of operating conditions. In the Pelamis primary transmission, high efficiency is maintained at low incident powers, which represent much of the available wave energy throughout the year [20].

2.2.2.2. Point Absorbers

Point absorber (PA) is a WEC which is a floating structure that oscillates with either one or more degrees of freedom. A PA usually moves either with respect to a fixed reference, or with respect to a floating reference [21]. A PA moves relative to its own components due to the wave action, where this movement is used to drive an electromechanical/hydraulic energy converter.

For a WEC device to qualify as a PA, their dimensions have to be significantly smaller than the prevailing wave length. As a general rule, to consider a WEC as a PA, its respective diameter should be between five to ten percent of prevailing wavelengths [22]. PA devices can be categorized according to the degree of freedom with which they capture the ocean energy. The next two subsections give a brief explanation of the respectively mode of capture.

2.2.2.2.1. Heaving systems
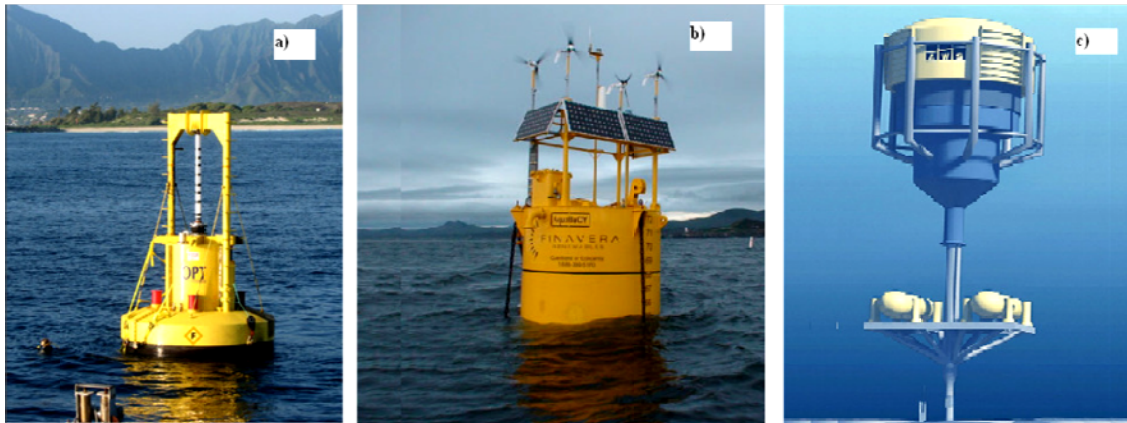
Figure 3. PA: (a) the Powerbuoy, (b) the Aquabuoy and (c) the AWS[2]

Heaving PAs are used to harness wave energy based on heave motion while the remaining movements are restricted by the mooring system which is fixed to the ocean bottom. During the past years, heaving PAs have been developed to capture wave energy because of the simplicity in their structure and similarity with the well-known buoys.

An example of a PA device is the PowerBuoy, developed by Ocean Power Technologies (Figure 3 (a)) [23]. This device consists of a floating structure with one immobile component, and a second component that moves with the respective wave motion (this is basically a floating buoy inside a fixed cylinder). The relative motion is used to drive hydraulic energy converters.

Another example is The AquaBuoy (Figure 3 (b)) [23] which was developed by the AquaEnergy Group Ltd. This is a PA that utilizes the wave energy to pressurize a fluid that is then used to drive a turbine. The vertical movement of the buoy drives a neutrally buoyant disk with a wide surface area, acting as a water piston within a long tube beneath the buoy. The piston motion in turn causes flexing motions in a hose containing seawater, and the change in the hose volume acts as a pump to pressurize the seawater.

Other PAs that have been undergoing some developments include the Archimedes Wave Swing (AWS) as shown in Figure 3 (c) [24]. This PA device is quite different compared to the ones described above. The AWS is a submerged structure which consists of an air-filled

---

[2] Image obtained online from a) http://subseaworldnews.com/2013/10/01/opt-tests-sonar-system-integrated-with-autonomous-powerbuoy/, b) http://teeic.anl.gov/er/hydrokinetic/restech/desc/wave/index.cfm, c) http://www.powermag.com/wp-content/uploads/2008/05/520004dd69dcc-48-02.jpg

cylinder that moves up and down as waves pass over. This motion is relative to a second cylinder fixed to the ocean floor which is in turn used to drive an electrical generator. An AWS with a capacity of 2 MW has been tested offshore in Portugal [25].

2.2.2.2.2. Pitching systems (PSs)

Another class of oscillating-body systems is pitching systems, in which energy conversion is based on relative rotation rather than translation. An example of such pitching systems include The PS FrogMk5 [26] which consists of a large floating paddle with an integral ballasted handle hanging below it as depicted in Figure 4 (a). Waves act on the blade of the paddle and the ballast beneath provides the necessary reaction. In these devices power is extracted by resisting the sliding of a power-take-off mass which moves above sea level.
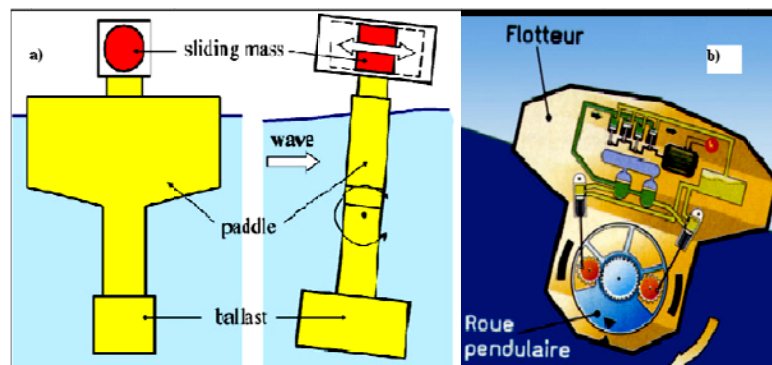
Figure 4. PA: (a) The PS FrogMk5, (b) The Searev and (c) The nodding Duck[3]

Other examples of PSs include the the Searev wave energy converter [27] shown in Figure 4 (b), developed at Ecole Centrale de Nantes, France, which is a floating device encapsulating a heavy horizontal-axis wheel serving as an internal gravity reference. In the Searev system, the centre of gravity of the wheel is off-centered so that this component behaves just like a pendulum. The rotational motion of this wheel activates a hydraulic PTO which in turn sets an electrical generator into motion. One of the most important advantages of this arrangement are that (1) all the moving parts are sheltered from sea turbulences inside a closed hull, and that (2) the choice of a wheel working as a pendulum means that it is virtually impossible to bring the system into a halt.

---

[3] Image obtained online from a) http://www.intechopen.com/source/html/42182/media/image38_w.jpg, b) http://nnmrec.oregonstate.edu/searev-point-absorber

2.3. General description of waves and currents

Water waves in general are the result of the oscillatory movements of a water surface caused by wind, tides, and storms. Waves are often characterized by their wave length L [m] or period T [s^{-1}]. A distinction can be made between shallow and deep water waves and is characterized by the ratio of the wave length to water depth h [m] and to the wave height H [m]. If $L \ll 20h$ one speaks of deep water waves [28].

Contrary to shallow water waves where the orbital motion of fluid particles is an ellipse, deep water waves are not affected by the bottom, and so the orbital motion of fluid particles follow a circular path. Figure 5 depicts the effect of the bottom on the orbital motion of waves. In this figure it is shown that for deep water the orbital motion of the waves does not reach the bottom and hence the waves are not affected by the bottom. However, the orbital motion of the wave is affected by the bottom as the waves are nearer to the shore. In the latter case, the waves feel the bottom and so the orbital motion of the wave particles become more elliptic [29].
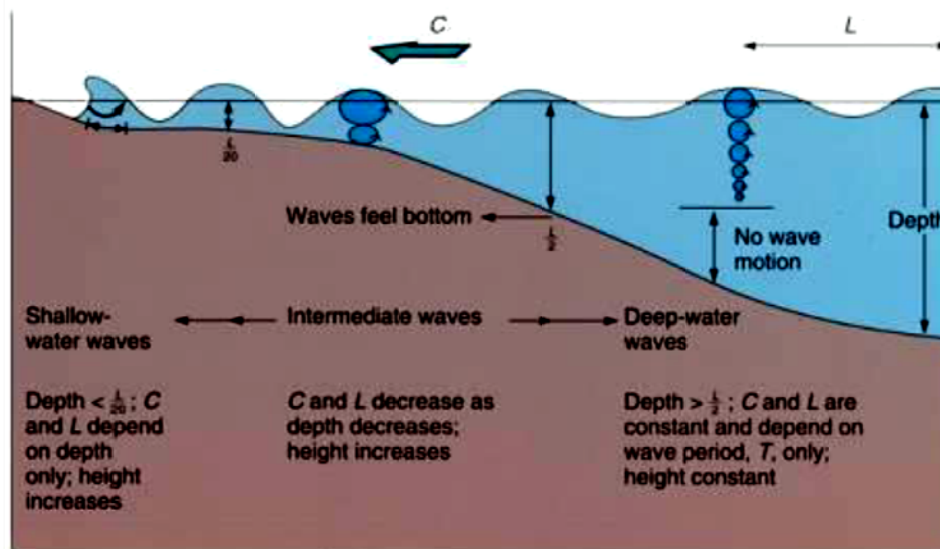
Figure 5. Changes in wave orbital motion as depth reduces [30]

2.4. Wave Energy Theory Description

Real ocean waves are described as random waves, which are composed of many waves of different frequencies, amplitudes and directions. It is possible to describe these wave parameters in terms of the directional wave energy spectrum $E(\sigma, \theta)$. The wave power level, J (W/m) in terms of the wave spectrum is:

$$J = \rho g \int_0^{2\pi} \int_0^\infty C_g E(\sigma, \theta) d\sigma d\theta \qquad (1)$$

In equation (1), ρ is the density of the seawater (1000 kg/m^3), g is the gravitational acceleration (9.81 m/s^2), C_g is the group velocity, θ is the wave direction and σ is relative frequency. Wave power computed using Delft3D-WAVE (which works according to SWAN) is formulated based on its x- and y-components:

$$J_x = \rho g \int_0^{2\pi} \int_0^\infty C_{gx} E(\sigma, \theta) d\sigma d\theta \qquad (2)$$

$$J_y = \rho g \int_0^{2\pi} \int_0^\infty C_{gy} E(\sigma, \theta) d\sigma d\theta \qquad (3)$$

where x and y are the geographical coordinates. Therefore, it is easy to calculate J [3]:

$$J = \sqrt{J_x^2 + J_y^2} \qquad (4)$$

The wave energy period (T_e) of the sea state and the significant wave height (H_s) are respectively given by:

$$T_e = 2\pi \frac{\int_0^{2\pi} \int_0^\infty \omega^{-1} E(\omega, \theta) d\omega d\theta}{\int_0^{2\pi} \int_0^\infty E(\omega, \theta) d\omega d\theta} \qquad (5)$$

$$H_s = 4 \sqrt{\int_0^{2\pi} \int_0^\infty E(\omega, \theta) d\omega d\theta} \qquad (6)$$

where $E(\omega, \theta)$ is the variance density spectrum and ω the absolute radian frequency determined by the Doppler-shifted dispersion relation.

In deep water areas, the wave power level per unit width of the progressing wave front in terms of the energy period and significant wave height can also be calculated by [31, 32]:

$$J = \frac{\rho g^2}{64\pi} T_e H_s^2 \qquad (7)$$

In SWAN, the evolution of the wave spectrum is described by the spectral action balance equation which for Cartesian co-ordinates is [3]:

$$\frac{\partial}{\partial t}N + \frac{\partial}{\partial x}c_x N + \frac{\partial}{\partial y}c_y N + \frac{\partial}{\partial \sigma}c_\sigma N + \frac{\partial}{\partial \theta}c_\theta N = \frac{S}{\sigma} \tag{8}$$

The first term on the left-hand side of this equation represents the local rate of change of action density in time ($N = E/\sigma$), the second and the third terms represent propagation of action in geographical space (with propagation velocities c_x and c_y in x- and y-space, respectively). The fourth term represents shifting of the relative frequency due to variations in depths and currents (with propagation velocity c_σ in σ-space). The fifth term represents depth-induced and current-induced refraction (with propagation velocity c_θ in θ-space). The expressions for these propagation speeds are taken from linear wave theory [3].

2.5. Wave induced currents

2.5.1. Longshore currents

Waves approaching a coastline at an oblique angle induce a mean current parallel to the coastline [33]. These longshore currents cause the sediments to be transported along the shore and so they influence the coastal morphology. Longuet-Higgins [34] derived a formulation of the longshore current based on his earlier research on radiation stress caused by waves [35].

If waves approach a uniform coastline along the shore under an angle, then a longshore current is generated. As waves approach the coast the energy in a wave is reduced due to wave breaking, which in turn causes a reduction in the wave generated radiation stress. Consider an area inside the surf zone as depicted in Figure 6, the cross-shore reduction of wave energy results in a smaller radiation stress towards the shore. The force induced by the cross-shore varying radiation stress on the water body is given by:

$$F_x = \frac{\partial S_{xx}}{\partial x} + \frac{\partial S_{xy}}{\partial y} \tag{9}$$

$$F_y = \frac{\partial S_{xy}}{\partial x} + \frac{\partial S_{yy}}{\partial y} \tag{10}$$

where, $F_{x,y}$ is the radiation stress induced force [N/m2].

According to the quadratic friction law, the cross-shore difference in radiation stress is compensated by a flow-induced bed shear stress:

$$\tau_b = \rho u_*^2 \qquad (11)$$

In which, τ_b is the bed shear stress [N/m2] and u_* is the friction velocity [m/s].

As the longshore current compensates the cross-shore gradient in the radiation stress, the magnitude of the longshore current is dependent on amount of energy dissipated by the waves and the roughness of the bottom. The rougher the bottom the lower the longshore current has to be to compensate for the gradient in the radiation stress.
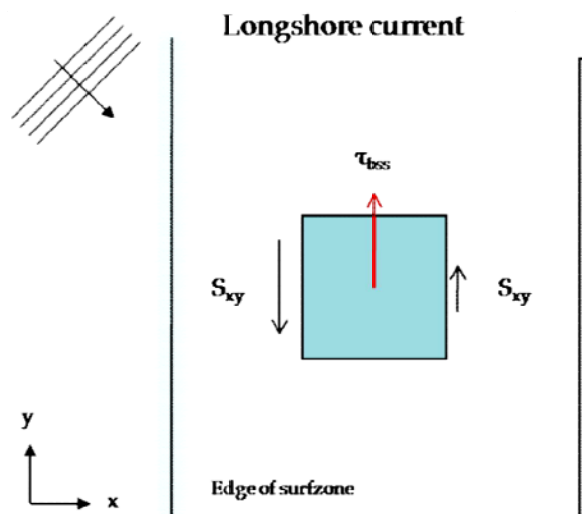
Figure 6. Radiation stress induced longshore current [36]

There does not occur any wave energy dissipation due to wave breaking occurs outside the surf zone and so both the wave energy and the radiation stress remain constant. However, due to the lateral exchange of momentum, a longshore current can still be generated just outside the surf zone. Battjes [37] has argued that, according to equation (12), the horizontal exchange of momentum induced by wave breaking, is dependent on the amount of wave energy which is dissipated:

$$v_t = h(\frac{D}{\rho})^{\frac{1}{3}} \qquad (12)$$

where, v_t is the horizontal eddy viscosity [m2/s], h is the total water depth [m], and D is the dissipation of wave energy [N/ms].

As depicted in Figure 7, due to the horizontal exchange of momentum, the cross-shore distribution of the longshore current resembles the distribution.
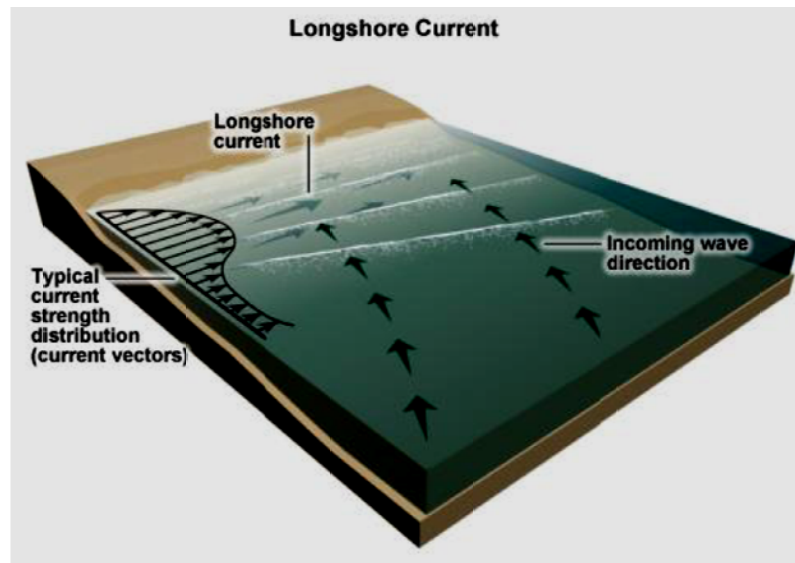
Figure 7. Sketch of wave-induced longshore currents [source: Meteorology Education and Training, by the University Corporation for Atmospheric Research (UCAR)]

2.5.2. Cross-shore current

As waves propagate towards the coast, the forward and backward displacement in the water is almost in balance. However, in the wave crest, there is a residual flux of water in the direction of wave propagation. As wave breaking occurs, the flux of water towards the land is enlarged since there is an additional flux of water in the form of a roller. Assuming that there are longshore-uniform conditions, landward discharge in the upper part of the water column must be compensated by an offshore directed return flow in the lower part of the water column [38].

Sediment transport is caused by the wave-induced cross-shore current since this current induces a directed bed shear stress component towards the direction of the sea which determines the rate of cross-shore sediment transport.

2.5.3. Tide induced currents

Tidal-induced are important for coastal engineers since the currents which they produce can cause important processes inside the surf zone. Similar to the waves, the tide induces a force on the water which affects the current velocity of the water near a coast. A tide is caused by the acting of the gravitational forces of the moon and the sun on the earth's water body and it

involves the cyclic horizontal and vertical movement of a water body. The magnitude of the effect of this gravitational force depends on several aspects such as regional bathymetry and such alike. Contrary to wind-induced waves, the tide is deterministic and predictable. The tide can induce large forces on a coastline and can sometimes be dominant over wave-induced forces [39].

2.5.4. Wind induced currents [40]

One of the most important goals of this thesis is to compute the wind-induced wave energy. This section briefly explains this type of waves.

A shear stress caused by the movement of air travelling over a body of water induces a force which causes the upper part of the water to move in the same direction as the wind. Once the wind reaches a certain threshold velocity, water ripples are developed on a calm water surface. The magnitude of this wind velocity depends on the vertical stability of the air as well as the degree of surface contamination. Seawater is always contaminated with various materials that tend to stiffen the water surface tension which means that greater wind speeds are needed to deform the surface (1.0-1.5 m/s, as measured 10 m above the water).

As the wind begins to blow, "capillary" waves controlled by the forces of gravity and surface tension are the first ripples to appear on calm water. These waves propagate at quite a low speed (i.e. 23 cm/s) and they form a "criss-cross" pattern of two sets of wave crests, where each set moves at an angle 70-80 degrees respective to the wind direction, with periods of 0.073 s, and with a spacing of about 1.8 cm between individual crests. There are two preferred directions for these ripples, one to the left and one to the right of the main flow of air along which the waves continually receive energy from the pressure fluctuations.

Frictional effects dampen the ripples and they quickly disappear if the wind dies, but if the wind becomes stronger, the heights, lengths, and periods of the ripples increase which in turn increases their propagation speed. The angle of wave travel with respect to the wind is then decreased, until there is a new gust of wind with speeds of about 2-3 m/s, where the wavelets start to move at 30 degrees relative to the wind.

Once the wind speed reaches above 3 m/s, the growing waves are independent of surface tension and their heights become large enough to affect the air flow. The water surface has now become "hydro dynamically rough" which in turn induces turbulent pressure fluctuations

in the wind, which eventually increase the amount of energy fed into the waves, and accelerate their length and height. With increased wind speeds above 3 m/s, the wave field becomes progressively more irregular as differences in the heights, lengths, speeds, and periods of the waves are continually increased by the wind. Furthermore, wave-wave interactions affect the transfer of energy from shorter to longer waves and the dominant wavelength increases.

Once the growth of wind-induced waves has progressed even further, beyond the so-called "capillary" waves, it is almost impossible to distinguish between individual wave groups. There now exists a continuous spectrum of waves, whose heights, periods, and so on, range from the smallest "capillary" wavelets, to the largest waves. It is extremely rare and virtually impossible to find well-defined wave patterns during intense winds.

2.6. Effect of water depth on the wave energy resource

Most of the recently proposed wave energy converters are planned to be installed in relatively shallow water depths where the wave energy resource is reduced compared to deep water [41]. According to [42], the average annual incident wave power reduces 27% at 50 m and 47% at 30 m compared to the deep water. Also, this work shows a significant reduction for both the wave energy resource and wave energy converted as the water depth decreases. Therefore, it is very important for us to study the effects of wave energy on water depth and vice-versa.

2.7. Delft3D general description

In this study only the Flow and Wave modules in Delft3D are used. These two modules can either be coupled – "online" or uncoupled – "offline". In the "online" mode (which is used in this study) there is an interaction between the Flow and Wave module at user defined intervals. The Wave module recalculates the wave conditions using the hydrodynamics from the Flow module at that certain interval. The newly updated wave conditions then are used as input for the Flow module (see Figure 8). In the "offline" mode there is no interaction between the Wave and the Flow module. The Wave module computes the wave conditions which are used as input in the Flow module (red-line). The interaction between Wave and Flow modules in online mode are explained completely in next chapters.

18
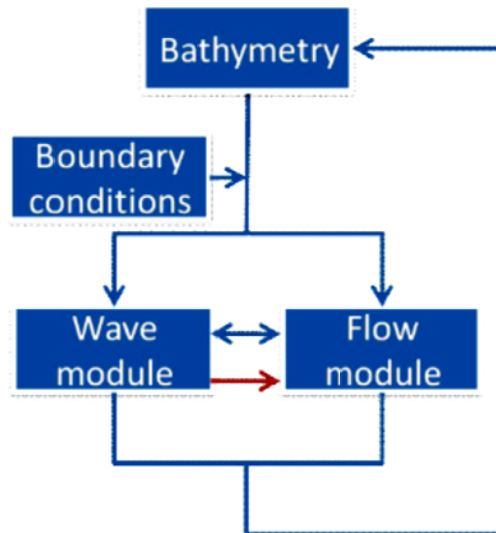
Figure 8. Delft3D computation scheme

For some processes such as wave deformation due to current and rip-currents, the online coupling between both modules is important since these processes are either the consequence or are enhanced by the wave-current interaction.

2.7.1. Flow module

The Flow module determines the hydrodynamics in Delft3D and describes the two-dimensional (2D) or three-dimensional (3D) unsteady flow phenomena. These are situations where the horizontal scale (length) are larger than the vertical scale (depth), for instance in coastal areas, shallow seas, estuaries, lagoons and rivers. A detailed description of the hydrodynamic formulas, assumptions, boundary conditions and numerical schemes used in Delft3D can be found in [43] and the Flow manual [44].

Delft3D-Flow solves the Navier-Stokes equations for an incompressible fluid under the shallow water and the Boussinesq assumptions. The vertical accelerations are neglected by assuming them small compared to the gravitational acceleration. The system of equations consists of the Continuity Equation and the Horizontal Equation of Motion.

When using the 3D approach, no vertical momentum equation is solved since the assumption is made that the vertical accelerations are small compared to the gravitation acceleration.

2.7.2. Wave module

The Wave module is used to compute the evolution of wind-generated waves in coastal waters (e.g. estuaries, tidal inlets, etc.). The Wave module computes wave propagation, wave generation by wind, non-linear wave-wave interactions and dissipation for deep, intermediate and finite water depths. In this study the wave model SWAN is used. SWAN, which is an acronym for Simulating Waves Nearshore, is based on the discrete spectral action balance equation and is fully spectral in all directions and frequencies. This implies that short-crested random wave fields that propagate simultaneously from all directions can be computed.

2.8. Background of the SWAN wave model

SWAN is a numerical wave model, used to obtain realistic estimates of wave parameters for given wind-, bottom- and current conditions, therefore the name: Simulating Waves Nearshore (SWAN). The SWAN model was developed by the Delft University of Technology [45].

2.8.1. Functionality of SWAN

The following propagation processes are incorporated in SWAN:
- Propagation through geographic space,
- Refraction due to spatial variations in bottom and current,
- Shoaling due to spatial variations in bottom and current,
- Blocking and reflections by opposing currents,
- Transmission through, blockage by or reflection against obstacles.

The model also accounts for the following generation and dissipation processes:
- Generation by wind,
- Dissipation by white-capping,
- Dissipation by depth-induced wave breaking,
- Dissipation by bottom friction,
- Wave-wave interactions (quadruplets and triads).

2.8.2. SWAN assumptions

As mentioned earlier, the main focus of this study is to develop a general description of the expected wave power conditions. The most direct method for obtaining the desired output from the simulation process is to conduct a SWAN simulation for each location in Portugal coast and then extract statistical parameters from the collective output. This exercise would be computationally expensive with at least 1 month required to simulate the entire data set. In order to reduce the number of computer simulations it was assumed that wave transmission is independent of wave height. This assumption is clearly unrealistic, but it will be shown later that the consequential discrepancies are marginal. This assumption significantly simplified the SWAN simulation process, in that wave height variation is only determined for boundary inputs of H_s and not for the entire range of H_s occurring in the entire data set.

There are three dissipation processes incorporated in SWAN that are dependent on wave height. These include:

1) **White-capping**

White-capping occurs when the maximum wave steepness of $H_{max}/L \approx 0.14$ is exceeded [29]. Energy dissipation due to white-capping occurs more frequently in the presence of wind fields and it is therefore expected that this dissipation process will have a small impact on the simulation output of this study.

2) **Depth-induced breaking**

Wave breaking due to wave-bottom interaction in shallower water and the consequential energy loss is incorporated in SWAN's surf-breaking source term (S_{surf}), with [29]:

$$S_{surf}(f,\theta) = D_{surf} \times E(f,\theta)/m_0 \qquad (13)$$

where $E(f,\theta)$ and m_0 are dependent on Hs inputs on the model boundaries.

3) **Bottom friction**

Energy dissipation through wave-bottom interaction is incorporated in SWAN by the source term as described below [45]:

21

$$S_{ds,b}(\sigma,\theta) = -c_{bottom}\frac{\sigma^2}{g^2 sinh^2(kd)}E(\sigma,\theta) \tag{14}$$

The source term for bottom friction ($S_{ds,b}$), is dependent on the energy density spectrum and therefore also dependent on H_s.

In the next section the actual wave transfer process will be discussed in detail with focus on the input requirements for the SWAN wave model.

2.8.3. Input requirements for SWAN model analysis

The first step in the simulation process is to define the computational area over which wave conditions are to be modeled.

2.8.3.1. Computational grid for SWAN simulations

In my study, a uniform, rectangular (regular) computational grid was specified for the SWAN simulation, which is made by Delft-Dashboard, because with this software, the user can make an exact and precise grid based on the map of the world. This grid contains part of the Portuguese coastal region.

Then the grid resolution was set. After the computational grid was specified, the next step was to prepare the other essential SWAN input parameters. These include:
- A bathymetry grid of the seabed inside the defined computational grid.
- Wave conditions on computational boundaries
- Boundary conditions to be prescribed in terms of wave parameter inputs at Base.

2.8.3.2. Bathymetric grid

Bathymetry data is existent in the Delft-Dashboard database, and can be used for computational grid which was explained before. This bathymetry data is precise and compatible with the computational grid and its resolution.

2.8.3.3. Boundary conditions

The final requirement for the simulation process is to prescribe the wave conditions on the boundaries of the computational grid. All the data for boundary conditions are obtained from

online databases as discussed previously. Wave conditions on the model boundaries are prescribed in terms of:

1) Peak wave period (T_e):

The wave period is an input condition which is prescribed in terms of T_e. The range of T_e for each boundary condition should be specified.

2) Peak wave direction (D_p)

The full directional spectrum of D_p ranging from 0 to 360° will be specified for each of the model boundaries.

3) Peak-enhancement factor (γ) and wave directional spreading (m)

The shape of the energy density spectrum and the directional spreading must be specified on the model boundaries. Associated distributions of these two parameters are presented in Figure 9 and Figure 10 shown below.
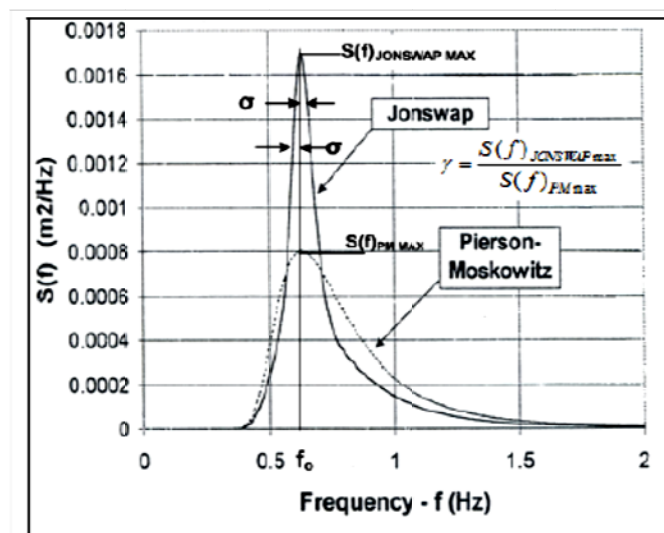
Figure 9. Peak-enhancement factor [46]
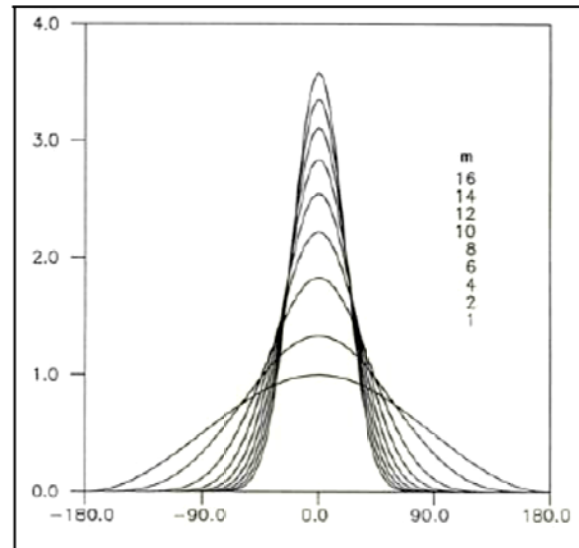
Figure 10. Directional spreading [47]

4) **Significant wave height (H_s)**

In order to initiate the simulation, wave height conditions in the SWAN model boundaries should be specified according to the online database. Whenever there was no data available, constant wave height conditions of 1m were assumed on the model boundaries and the software also estimates initial values for T_e and D_p (called the base data set). These assumptions generally have little impact on the final result of the study due to the small probability of occurrence of the T_e and D_p combinations in the base data set. The SWAN wave model interpolates linearly between prescribed values on the model boundaries in order to determine the wave conditions at each boundary grid point.

In SWAN applications wave conditions on the model boundaries are often unknown. No wave inputs or uniform conditions are assumed along such boundaries. These erroneous boundary conditions are then propagated into the model. To overcome this complication the computational grid is specified in such a way that the area of interest is far away from the model boundaries.

In this study, wave conditions at certain boundary grid points were known and prescribed as determined by online database. These prescribed conditions are reasonable estimates of actual wave conditions and are more realistic than assuming no or uniform boundary conditions.

2.9. Delft Dashboard

Delft Dashboard (DDB) is part of Open Earth Tools, and is a standalone, MATLAB-based software. DDB provides a graphical user interface that supports the user in the setting up of a new model or in altering an existing model. It is currently fully integrated with Delft3D Flow. DDB provides an easy access to many online databases through "Open-source Project for a Network Data Access Protocol" (OPeNDAP).

Although the DDB is MATLAB-based, one does not need to have MATLAB installed. However, MATLAB runtime libraries, which are freely made available by Mathworks must be installed. Instead of the DDB binaries, one may decide to download the MATLAB source code for the DDB and use the software directly through MATLAB. To do this, the user must first download The Open Earth Tool (OET).

3. Delft3D-based Model Used for Verifying the Proposed Method

Delft3D is a software package that was designed primarily as an application focused on water flow and quality. The package consists of several modules coupled together to provide a complete picture of three-dimensional flow, surface waves, water quality, ecology, sediment transport and bottom morphology in complicated, coastal areas. This software package has three main simulation models: Flow, Wave and Flow with online Wave simulation. The Flow with online Wave simulation which is used in this work is the most accurate simulation, because it incorporates the effects which waves, currents and sediment transportation have on each other as well as on the morphology of the seafloor.

As explained in Chapter 2, DDB is a standalone MATLAB-based graphical user interface in order to set up new and existing models. It allows a model to be set-up in a matter of minutes for every location in the world, which would otherwise take days or weeks to model manually if even possible at all. Different online and offline data sources are included in this software for making seawater bathymetry files.

To simulate wave parameters, the third generation wave prediction model was executed in a two-dimensional and non-stationary manner. The spectral space was resolved in 36 directions and 24 spaced frequencies between 0.04 Hz and 1 Hz. Quadruplet nonlinear interactions, depth-induced wave breaking and bottom friction and diffraction were activated in the execution. The open boundary conditions and wind parameters for Matosinhos were obtained from the output data of the Magicseaweed online database. Magicseaweed obtains its measured and boundary conditions data from NOAA measured database[4]. The nearest buoys which are used by NOAA for Portugal were located at 47.500 N 8.500 W, 45.201 N 5.000 W and 48.701 N 12.401 W. The initial hydrodynamic conditions of computational areas were set using DelftDashboard. Also, the model is implemented on nautical coordinates.

The simulation time is classified into three different parts:

- First, it covers 3 days, from 8th of April 2013 until 11th of April 2013. The model is run with 2-minute time steps and the simple boundary condition (i.e. an initial

---

[4] For more information see website, http://magicseaweed.com/Magicseaweed-Data-Sources-Article/321

boundary condition which is given as input to the software to get it running) is used for the first instance. A rectangular grid system is adopted in this model which consists of 930 grid points near the Matosinhos.

- Second, the simulation time covers 7.5 days, from 29 September until 6 October 2013. This time, the same model with the same grid points and bathymetry is run with 15-minutes time step and time-varying boundary condition (5 different times, i.e. boundary conditions are provided for every 1.5 days) in order to have accurate results.

- Finally, the validation of this method is studied for the same computational area during 25 days, from 30 August until 24 September. In the third simulation, time step is 30 minutes and time-varying boundary condition (20 different times, i.e. boundary conditions are provided for every 1.25 days) is used.

3.1. Method validation for first simulation model (3-day simulation with a simple boundary condition)

In the present work, the wave energy density obtained from the wave model simulation in Delft3D was used to determine where this value was large enough in order to establish the potential sites where the energy can later be used to generate electricity. However, at first, the model accuracy had to be verified. Figure 11 shows the six stations (dotted in black) where wave parameters are collected. The scale column on the right hand side of the figure depicts water bathymetry. All six stations are included in the Matosinhos computational area.
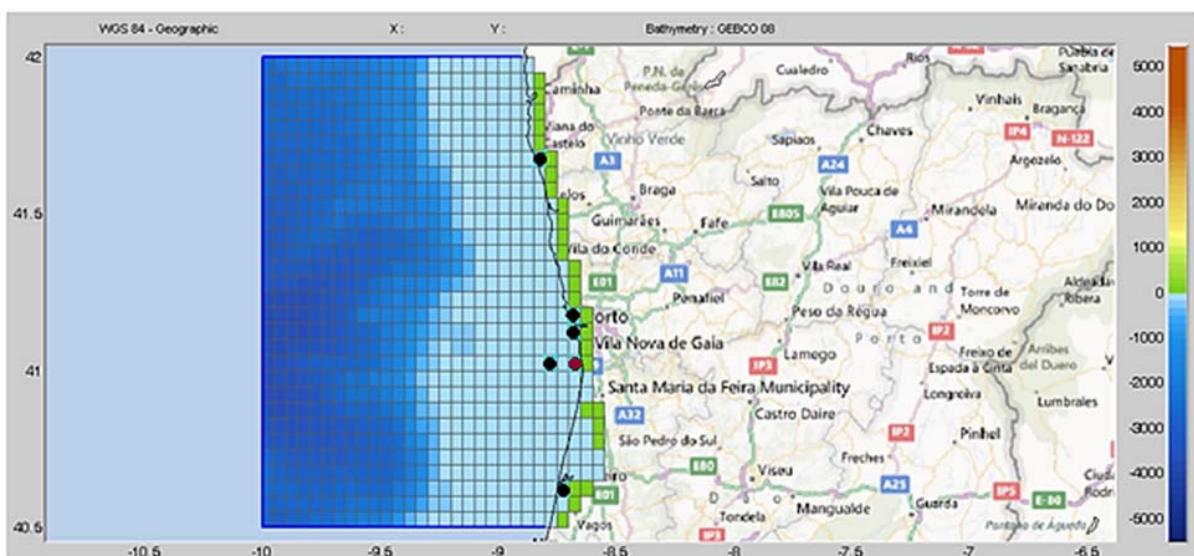
Figure 11. The Matosinhos computational area (dotted in black are wave observation stations and the red dot represents the Matosinhos observation point)
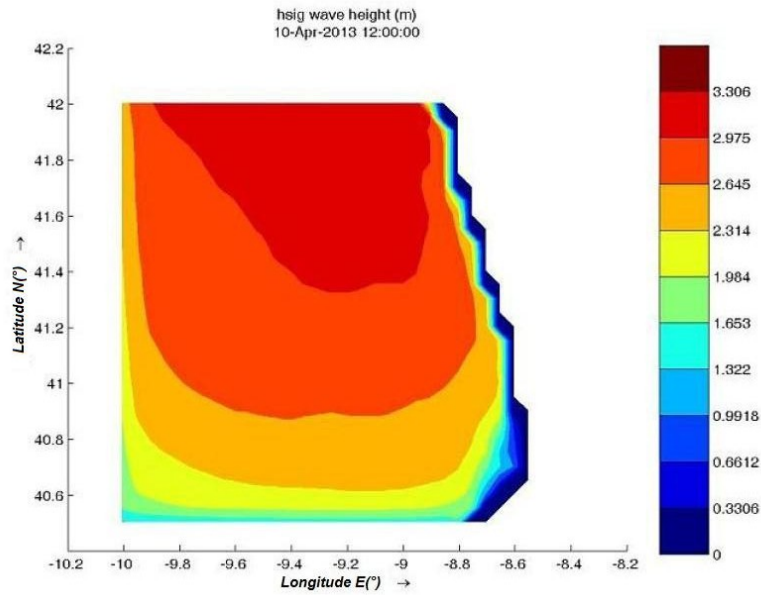
Figure 12. The largest significant wave height around Matosinhos during 3 days

Figure 12 shows the distribution of the largest significant wave height around Matosinhos within 3 days. According to this figure, it is clear that the offshore waves are much stronger than the nearshore ones, making them a suitable candidate for implementing wave convertors in this region.
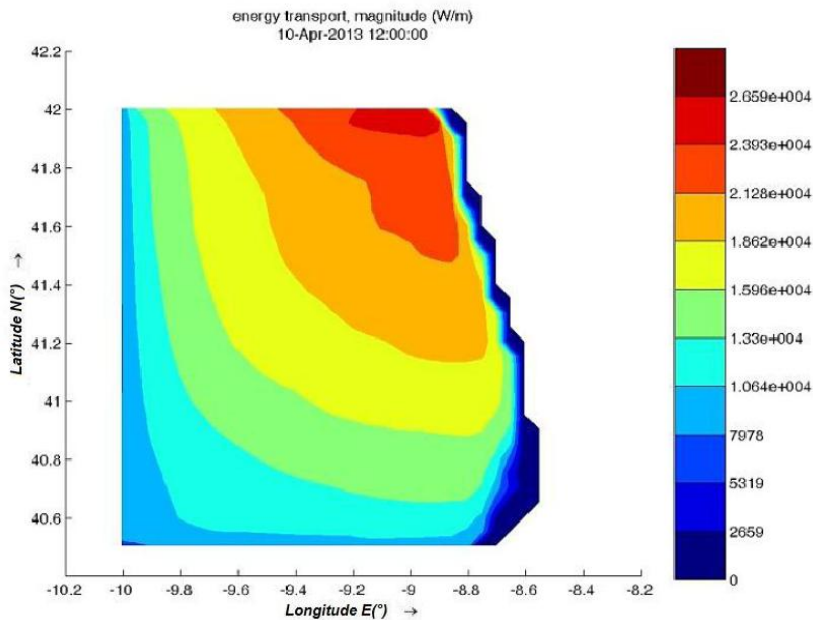
Figure 13. The largest wave energy density around Matosinhos during 3 days

Figure 13 depicts the largest wave energy density around Matosinhos over a simulation period of 3 days. Based on this figure, the largest wave energy density occurs at 27 kW/m

under the influence of vigorous waves occurring in the northeast offshore zones of the Matosinhos headland.

Finally, measured data collected from Magicseaweed online database are compared with the Delft3D model data in order to verify the proposed method of wave energy calculation. As depicted in Figure 14, there is a relatively good agreement (89.42%) between the significant wave height data obtained from the given model and those of the online measured database. Hence, it can be concluded that the suggested method can predict wave energy accurately. Also, the correlation between the modeled and the measured data is 0.807, a value which can be improved by using time-varying boundary condition instead of a simple one.

To compare the results, the following statistical formulas were used:

$$agreement = \frac{1}{n} \sum (1 - \frac{|h_{msi} - h_{mdi}|}{h_{msi}}) \times 100 \tag{15}$$

$$correlation\ coefficient = \frac{\Sigma(h_{msi} - \overline{h_{ms}})(h_{mdi} - \overline{h_{md}})}{\sqrt{\Sigma(h_{msi} - \overline{h_{ms}})^2 \Sigma(h_{mdi} - \overline{h_{md}})^2}} \tag{16}$$

Where h_{msi} represents the measured significant wave height data and h_{mdi} represents the modeled significant wave height data. Also, $\overline{h_{ms}}$ and $\overline{h_{md}}$ are the mean value of measured and modeled data respectively, and n is the total number of data.
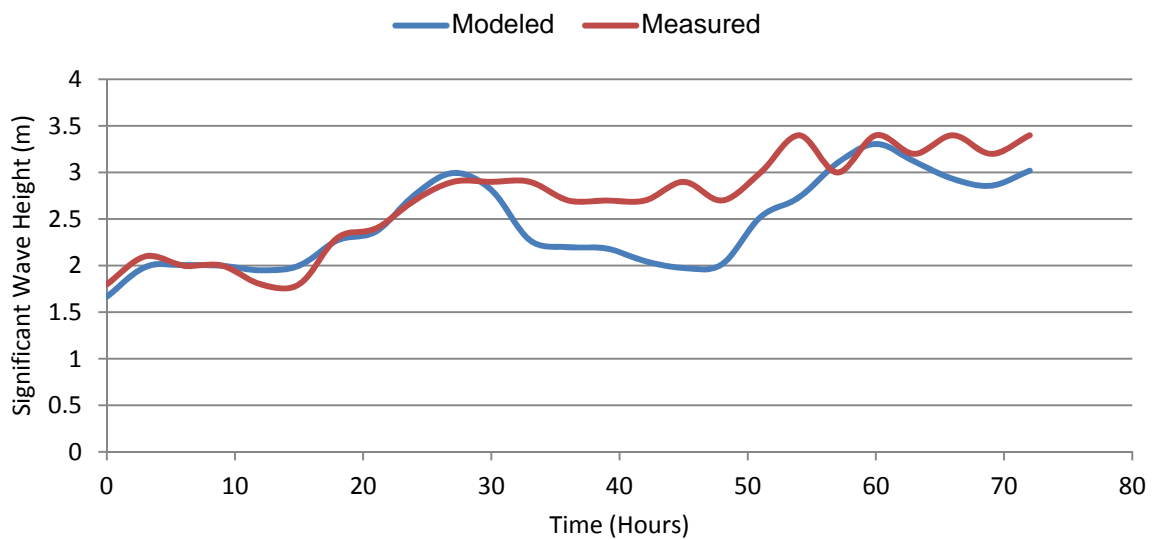
Figure 14. A comparison between the model and the measured significant wave height during 3 days in Matosinhos (simple boundary condition)

3.2. Method Validation for second simulation model (7.5 days simulation with time-varying boundary condition)

The wave model is surrounded by five boundaries. The model has north, northwest, west, southwest and south boundaries at which boundary conditions have to be prescribed. This time unlike the last simulation, these boundaries were forced by 5 time-varying wave spectra in order to have accurate results with a good correlation between measured and modeled data. Also, to gain reliable wave calculation, it was essential to select an appropriate input wind field because the results of any numerical wave study depend on the quality of the wind data. Therefore, a measured wind field integrated with the meteorological stations near the shoreline was used as the wind input in the wave model. The wind data in the computational area has been recorded with three hours interval.

A qualitative view of the calibration result for the time-varying boundary condition model, in terms of significant wave height is illustrated in Figure 15. As it can be seen, there is a very good agreement (86.08%) and a good correlation (0.86) between the model results and measurements.

Figure 15. A comparison between the model and the measured significant wave height during 7.5 days in Matosinhos (time-varying boundary conditions)

3.3. Method validation for the third simulation model (25-day simulation with a time-varying boundary condition)

This time, the same model with the same grid and bathymetry was used in order to investigate the accuracy of the model in the long term. According to Figure 16, the agreement (80.08%) and correlation (0.89) between measured and modeled results are high similar to the previous ones. However, the reason that there is less agreement between measured and modeled results this time is that ocean waves were too steady and short during eight days of simulation time (30, 31 August and 1, 3, 4, 9, 12 and 13 September 2013). So, during these days, any small difference between modeled and measured results made a big difference in the agreement.

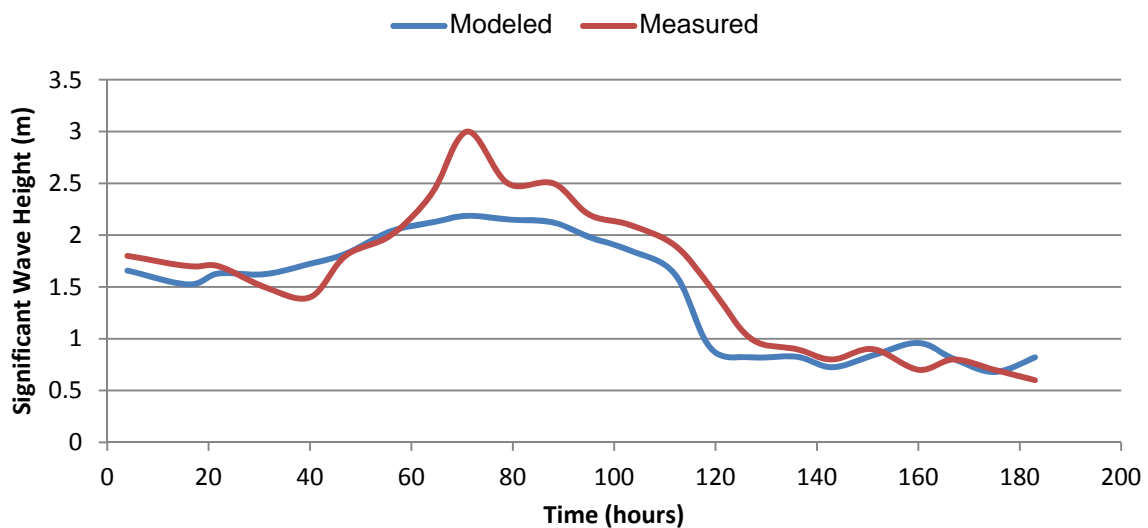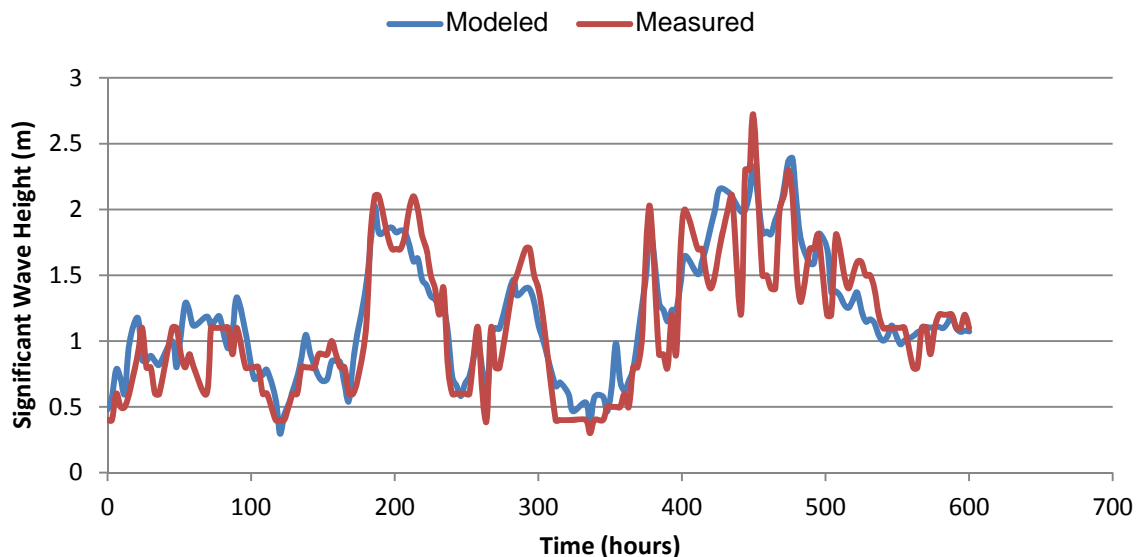**Figure 16. A comparison between the model and the measured significant wave height during 25 days in Matosinhos (time-varying boundary conditions)**

Based on the proposed method, three further computational locations in different grid points for the North model are chosen to investigate the potential wave energy resources in detail. The results obtained from these locations will be explained fully in the following chapters.

4. Making of the Second Model and Extracting Input Data for Two Models

After validating the method, in order to have the most accurate results, two small models (the previous one (based on the northern part of the Portuguese western coast) and the second model (based on the southern part of the Portuguese western coast)) are simulated for the Portuguese western coast in this project because more accurate results are obtained with two small models instead of one big computational grid (since there exist two extra boundary conditions when there are two small models compared to the single model).

The longitude of the first model (Figure 11) is between approximately 40.5 and 42 degrees and the longitude of the second model is between 40.6 and 37.3 degrees. So, these two models cover the Portuguese western coast almost completely.

Figure 17 shows the second area and six stations (dotted in black) where wave parameters are collected in the second model. The scale column on the right hand side of the figure depicts water bathymetry and the axes represent geographic latitude and longitude.
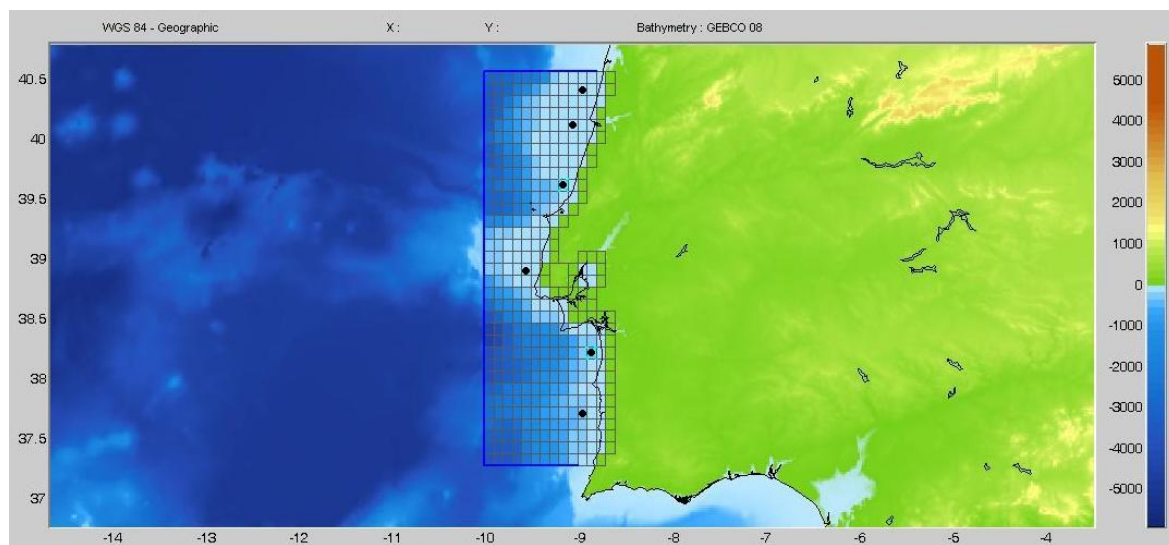
Figure 17. The south part of Portuguese western coast computational area (dotted in black are wave observation stations)

To find the high potential locations of wave energy, the changes of wave energy in the observation points of these two models are compared with each other in the period of 25 days which was between 30 August until 24 September 2013.

For boundary conditions, data are given to Delft3D software according to the orientation in

the computational grid. In these two models, five boundaries (north, south, west, southwest, and northwest) are made and in each of these boundaries, 25 boundary conditions (time varying boundary conditions) are defined according to the buoy data which was explained in Chapter 3. Tables 1 and 2 show the buoy data which were gathered for boundary conditions of the western boundary of the models. Other results for north and south models are gathered in the Appendix.

Table 1. Boundary conditions for west orientation of south model (Figure 17)

Date (yyyymmdd)	Significant Wave Height	Wave Period	Wave Direction (°)
20130830	0.1	16	305
20130831	0.5	11	304
20130901	0.8	8	333
20130902	0.6	9	307
20130903	0.2	6	332
20130904	0.3	14	293
20130905	0.6	11	294
20130906	0.6	10	294
20130907	1.7	9	323
20130908	1.8	8	329
20130909	1.5	7	339
20130910	1	14	333
20130911	1.2	7	325
20130912	0.2	9	291
20130913	0.3	5	310
20130914	0.4	7	342
20130915	0.4	15	332
20130916	0.3	11	324
20130917	1.5	7	328
20130918	2.4	12	332
20130919	1.7	8	336
20130920	1.1	11	331
20130921	1.4	9	326
20130922	0.3	10	348
20130923	0.8	14	320
20130924	0.7	12	290

Date (yyyymmdd)	Significant Wave Height	Wave Period	Wave Direction (°)
20130830	0.3	11	312
20130831	1.1	11	311
20130901	0.8	10	300
20130902	0.8	13	308
20130903	0.8	11	314
20130904	0.4	9	319
20130905	0.8	11	286
20130906	0.6	10	286
20130907	1.8	11	307
20130908	2	8	323
20130909	0.6	9	322
20130910	0.4	10	300
20130911	1.7	8	322
20130912	0.2	10	283
20130913	0.2	12	295
20130914	0.6	13	296
20130915	0.8	10	299
20130916	1.7	11	317
20130917	2	7	322
20130918	1.5	12	315
20130919	1.2	11	319
20130920	1.2	11	309
20130921	1.5	9	315
20130922	1.1	9	309
20130923	1.1	11	299
20130924	1.2	11	273

For wind data, the averages of wind speed and wind direction of three different locations of the two models are calculated (i.e. the north, center and south of each computational area). For both wind and wave data, nautical and Cartesian system can be used, however, in this work, nautical system was used because our entire model making was based on the nautical system. Figures 18 and 19 show the results of these calculations for wind speed and direction in both models.
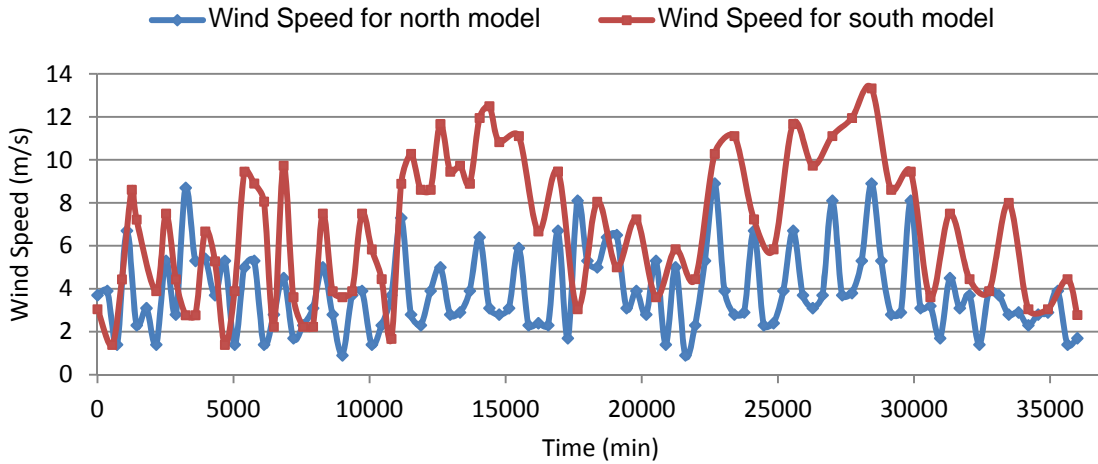
Figure 18. Wind speed during 25 days in the North and South models of Portuguese western coast
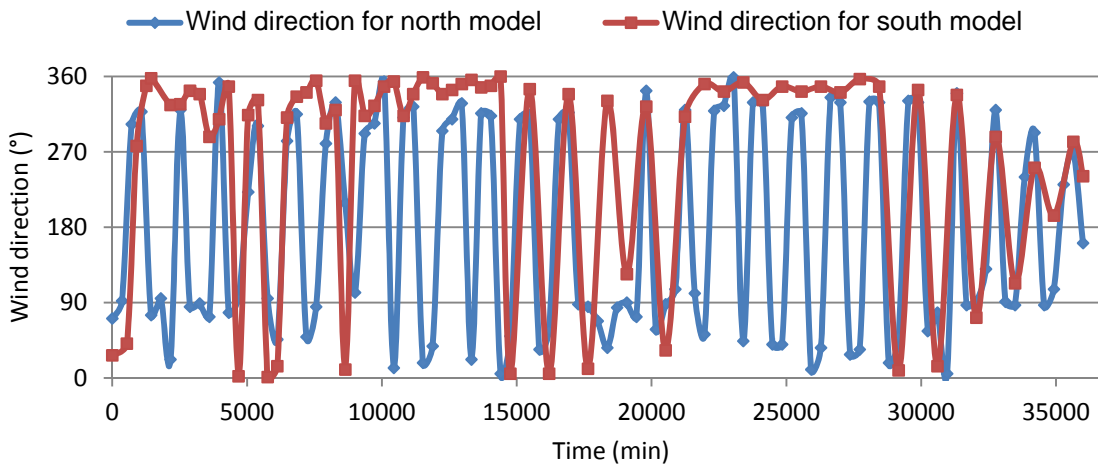
Figure 19. Wind direction during 25 days in the North and South models of Portuguese western coast

The grid which was used for the second model (southern part) like the northern part was a rectangular grid and it contained 16 cells along the x-direction (M) and 35 cells along the y-direction (N). Also, some other physical parameters had to be defined for both models. These constants included:

• Gravity = 9.81 m/s^2

• Water density = 1000 Kg/m^3

• North (direction with respect to the x-axis (Cartesian convention) = 90°

• Minimum depth (threshold depth in m; any positive depth smaller than [dep$_{min}$] is made equal to dep$_{min}$ = 0.002 m

• Convention = nautical for wind and wave direction. The direction of the vector from geographic North measured clockwise $+180^o$ (the direction where the waves are coming from or where the wind is blowing from)

• Setup: No this option should be used only if SWAN is used on standalone mode or if wave-induced setup is not accounted for in the flow computations. The wave-current interaction is required to account for the morphological changes of the model, which prevents the use of the setup option

• Forces: The wave forces are computed on the basis of wave dissipation rate, not on the gradient of the radiation stresses tensor, which is also another option

Furthermore, output parameters had to be defined correctly in Delft3D. In the data group's Output Options, I was able to specify which computational results could be stored for further analysis or for other computations and which output could be printed. Delft3D modules use one or more Map, History, Communication and Restart file to store the simulation results and other information needed to understand and interpret what is on the files.

Maps are snap shots of the computed quantities of the entire area. As we (can) save all results in all grid points a typical Map file can be many hundreds of megabytes large. So typically, Map results are only stored at a small number of instances during the simulation. In a History file, all results could be stored as a function of time, but only in the specified monitoring points. The amount of data is usually much smaller than for a Map file and history data are typically stored at a small time interval to have a smooth time function when plotting the results.

After defining all parts of the input data for the two models, wave and flow modules run with each other in a cycle called Delft3D-Mor. This module starts the processes, activates and de-activates process controllers and modules, takes care of the data communication between the modules and stops the process simulation. In Delft3D-Mor, the updated bed levels are used by the hydrodynamic module to update the wave and flow fields (i.e. a morphodynamic simulation).

The Waves and Flow modules are executed together in one loop to take the effects of wave-current interaction into account.

Based on the hydrodynamic data, the Transport and Bottom modules are executed a number of times by applying the continuity correction. When a user-specified maximum bed level

change has been computed, the hydrodynamic module is executed again with the most recent bed level to update the wave and flow fields. For all time steps, the wave quantities (wave height, direction, etc.) are computed within one call to the Waves module. The results are written to the Waves data group on the communication file, together with the time steps. Within one call to the Wave module, the Wave module uses the most recent bed level available on the communication file, and this cycle between wave and flow modules and transport and bottom modules is repeated until the last time step. The cycle is shown in the Figure 20. The changes in water depth level obviously have an important effect on the significant wave height and as a result, it can change the amount of wave energy. So, in order to have the most accurate results, the Flow, Wave, Transport and Bottom modules should be considered at the same time.
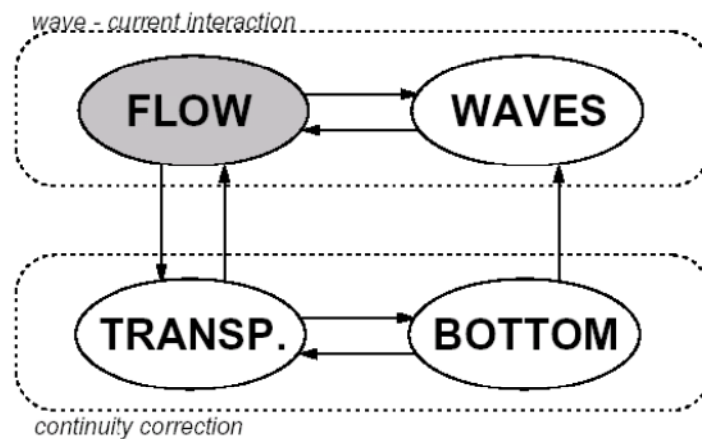
Figure 20. Schematic overview of a morphodynamic simulation (Extracted from the Delft3D-MOR Manual)

5. Results and Discussion

5.1. Wave energy resources

When the wave farm is constructed, location with a high potential for wave energy could be identified. First, the nominated locations should be chosen. In this work, two important factors have been considered for choosing these locations: First, they should be near a coastal city in Portugal and second, these coasts must not be rocky, so that the extraction of wave energy is feasible. Also, in choosing these locations, the entire coast of Portugal has been considered.

So, according to these factors, 5 sites in the southern part of the Portuguese western coast were chosen (see black dots at Figure 17, exclude the first one from top): Figueira da Foz (40.15 N, 8.85 W & M: 11, N: 30), Cascais (38.7 N, 9.42 W & M: 6, N: 15), Sesimbra (38.71 N, 9.18 W & M: 11, N: 12), Peniche (39.35 N, 9.36 W & M: 7, N: 22) and Sines (37.93 N, 8.77 W & M: 12, N: 8) and also, 4 sites (black dots in Figure 11, exclude the third one from top) in the north including: Viana do Castelo (41.7 N, 8.83 W & M: 23, N: 25), Leixoes (41.18 N, 7.8 W & M: 26, N: 15), Matosinhos (41. 18 N, 8.68 W & M: 26, N: 12) and Aveiro (40.63 N, 8.65 W & M: 25, N: 4) were chosen. The first part of these parentheses shows the geographical latitude and longitude of the locations and the second part (MN) shows the x-y location of these locations in their grids (North model or South model).

After selecting the area with the largest potential for a wave farm, in order to find the places with the highest potential for wave energy extraction in the northern and southern part of the Portuguese western coast, the wave energy variation of these sites during this 25 days (between 30 August and 24 September) with the input data which was discussed in the previous chapter were studied.

Figures 21 and 22 show the wave energy magnitude in the 9 nominated locations. According to these figures, the highest wave energy magnitude in the south model can be seen in Cascais, and Viana do Castelo has the highest wave energy magnitude in the north model. The detailed results of these two locations are investigated precisely. Also, the trends of the two models are similar to each other as expected, and all locations have the highest wave energy magnitude on 17 September. Furthermore, the amount of wave energy during

September in these locations which exceeds 50 kW/m in Cascais shows that the Portuguese western coast has large wave energy resources in itself.
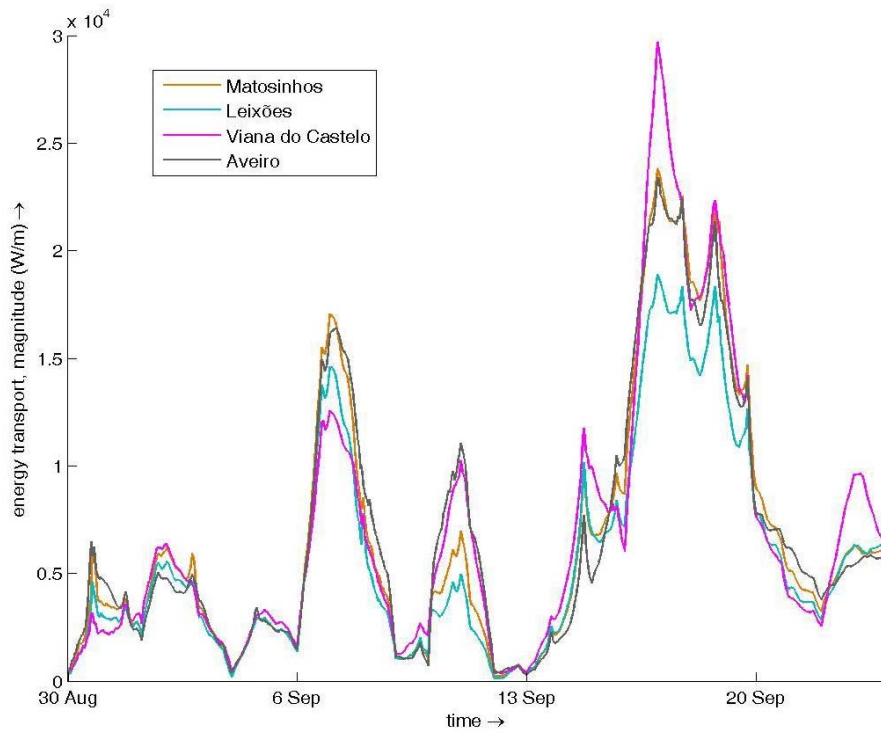
Figure 21. Wave energy transport magnitude in the North part of the Portuguese western coast
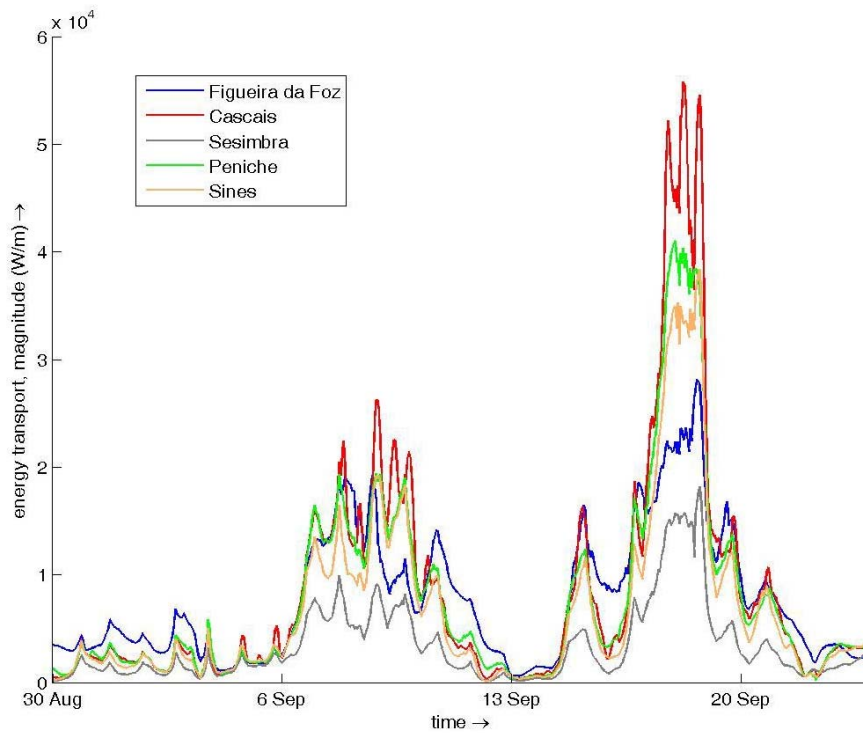
Figure 22. Wave energy transport magnitude in the South part of the Portuguese western coast

Figures 23 and 25 show the distribution of the largest significant wave height in the north and south model within the computed 25 days. According to these figures, it is clear that the offshore waves are stronger than the nearshore waves. The largest offshore significant wave height in the north model is 3.3 m and this magnitude in the south model is 4.3 m. However, the largest nearshore wave height in the north model is 2.5m and in the South model it is 3.4m. Moreover, the wave height in the north model decreases from north to south and west to east gradually and also, it decreases from south to north in the south model. Around Cascais, the largest significant wave height is 3.3 m, and around Viana do Castelo, this amount is about 2.4 m.

Based on the figures 24 and 26, the largest wave energy density in the north model occurs in the northwest (NW) offshore zones of the Portuguese western coast, which is 52 kW/m within the 25 days, and in the South model, the largest wave energy occurs in the center of the model near the Cascais which is 57 kW/m. The largest values of wave energy density like the significant wave height occur in the offshore areas. However, this amount in the nearshore areas of the north model is about 33 kW/m and in the south model, it is about 40 kW/m.
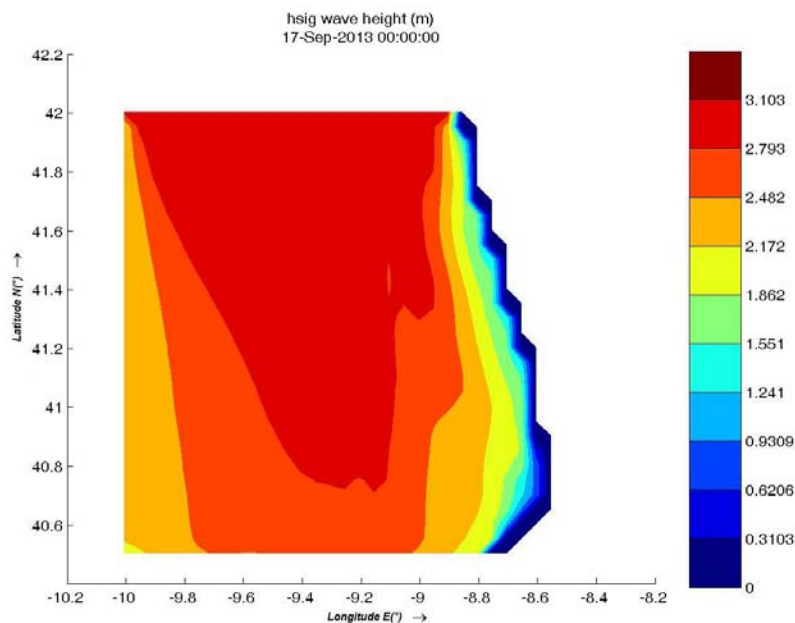
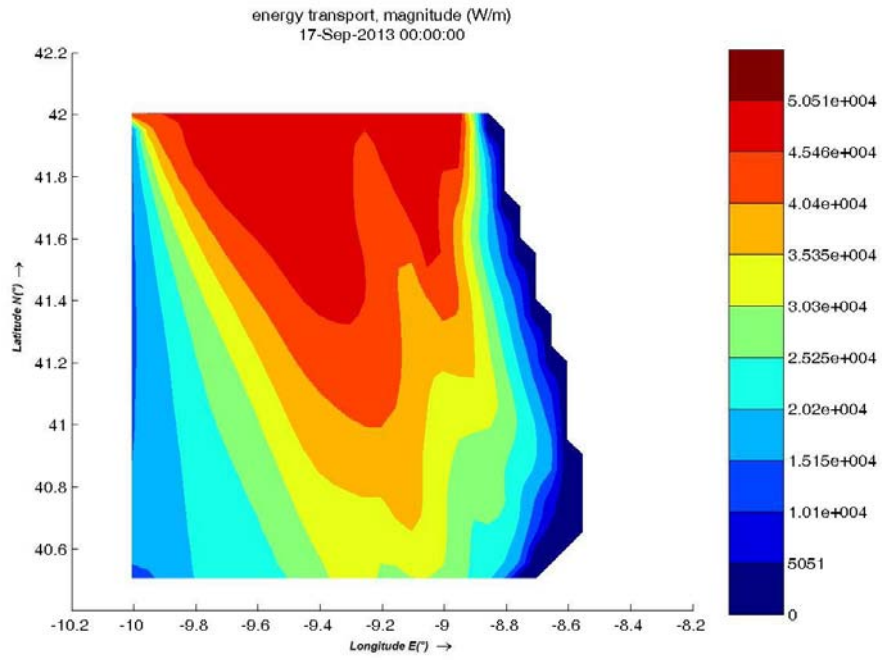**Figure 23. The largest significant wave height during 25 days in the North model**

Figure 24. The largest wave energy magnitude during 25 days in the North model
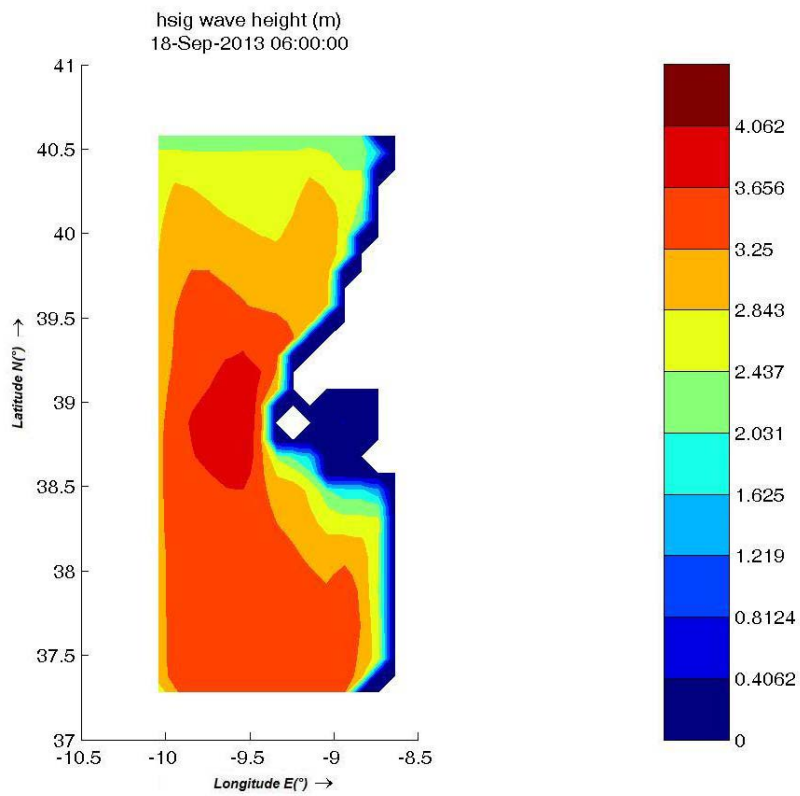
Figure 25. The largest significant wave height during 25 days in the South model
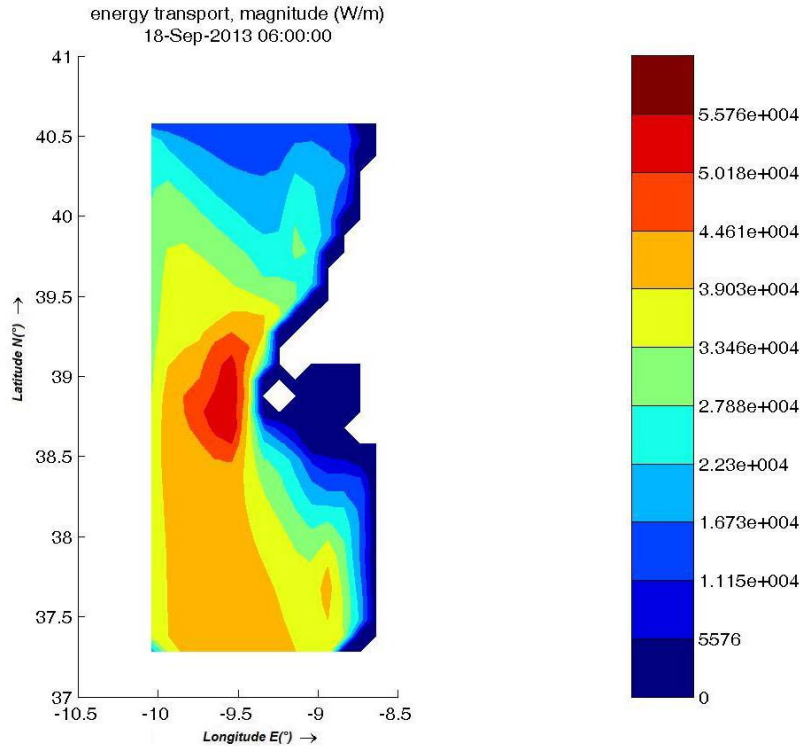
Figure 26. The largest wave energy magnitude during 25 days in the South model

As I mentioned before, in this work, the Flow and Wave module work together. So, for the entire period, Flow ran continuously interrupted only by the hourly run of the Wave module. This mode allowed for the input of time series of water levels and wind inputs. The Wave module can interpolate from the spectra input and it can keep its continuity using Restart files. So, water depth changes in every grid point in each run of Delft3D. Also, the 9 wave energy potential locations were chosen based on section 2.6 which explained about the water depth and that wave energy extraction can be feasible in the water depth between 30 m and 90 m. Figures 27 and 28 show that the water level changes in the 9 locations during the computation period. In section 2.6, the extreme effect of the water level in the nearshore areas on the wave energy were discussed. So, it is so important to consider the effect of the water level, Flow module, Wave module and sediment transportation on each other at the same time.
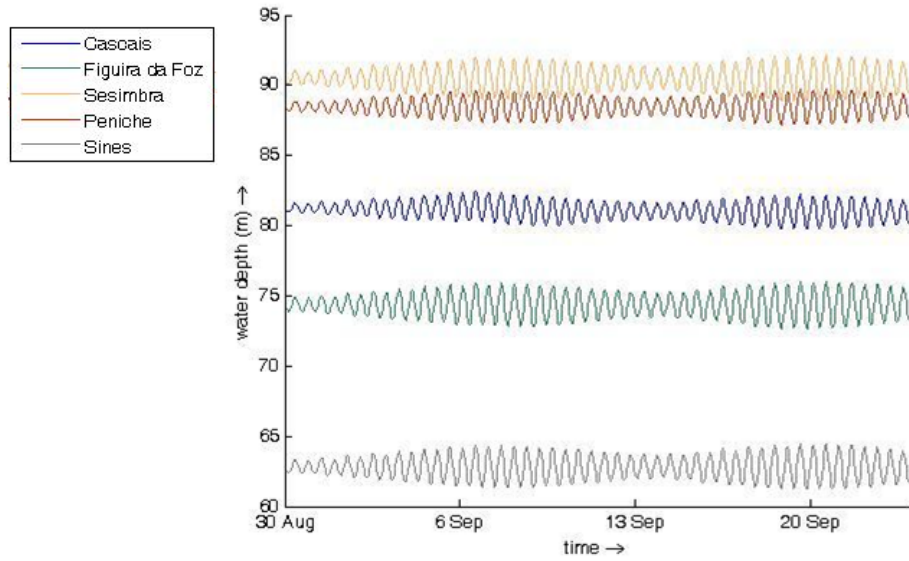
Figure 27. Water depth change during 25 days in the South model locations
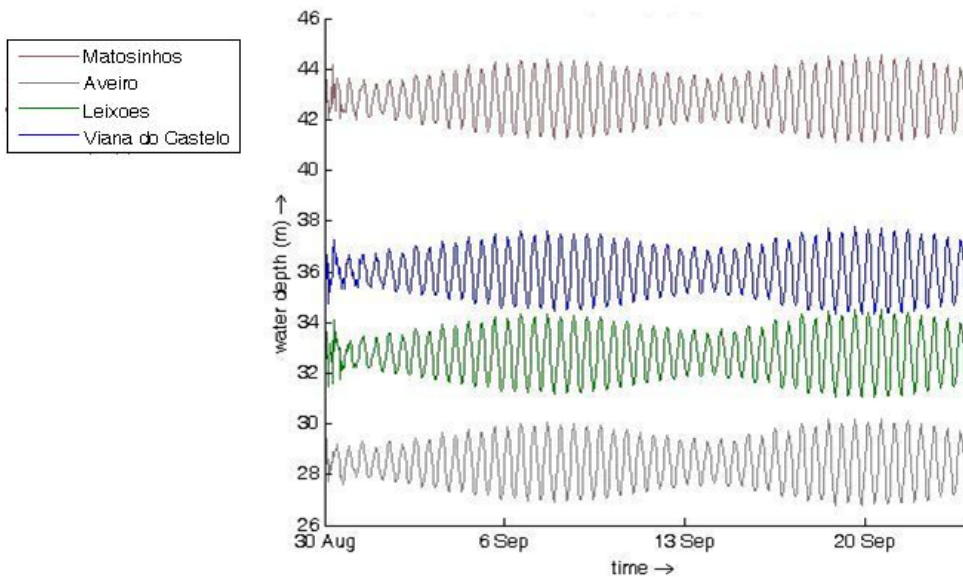
Figure 28. Water depth change during 25 days in the North model locations

5.2. Wave energy scatter diagram

The wave energy scatter diagram is a figure showing the frequency of occurrence of wave states and the combinational wave power of H_s and T_e values. The most dominant H_s and T_e combinations can be identified using a scatter diagram. This information is crucial to figuring out the efficiency in power extraction of WEC units. The power extraction efficiency of WEC units can be predetermined by comparing the dominate wave conditions and consequent available wave power resource to the performance curves of WEC units. In order

to produce a scatter diagram, the following procedure was followed for each (data-collecting) station's wave data:

a) Determination of the number of combined H_s and T_e recorded data.

b) Determination of the amount of power generated by each concurrent H_s and T_e value.

The wave energy scatter diagram for Vianda do Castelo station in Figure 29 indicates that the most frequent and powerful T_e and H_s values range between 8-10 s and 1-2 m respectively. The range for the latter wave condition produces a total energy of approximately 0.9 MWhr/m during the computational period. An important fact to be stated is that the highest number of occurrence of waves being produced which is recorded as 121 as shown in Figure 19 (with H_s between 1-2 m and T_e between 6-8 s) does not necessarily entail the highest wave energy. In figures 19-27, the color scale represents the total wave energy per meter during the computational period (25 days), and the bold numbers indicate the number of wave states occurring within the time which the state occurred during the number of hours per computational period. The results are based on a 25-day (601 iterations) run of the software.
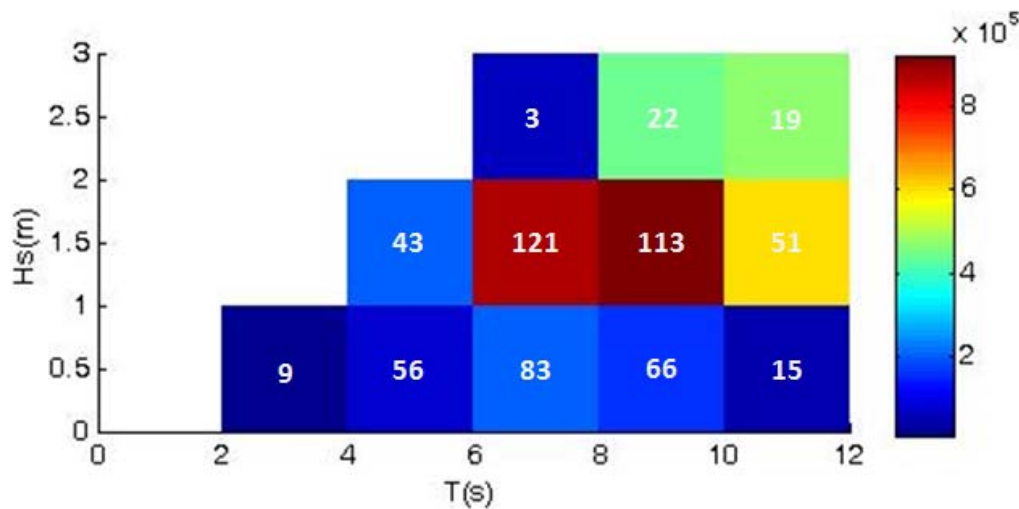
Figure 29. Combined scatter and energy diagrams of Viana do Castelo in different ranges of H_s and T_e

Similar to Viana do Castelo's data-collecting station and according to Figure 30, Leixoes's most dominant T_e values range from 8-10 s. The associated peak energy is approximately 1.6 MWhr/m during the 25 days. This is higher than the peak energy of Viana do Castelo, due to the fact that the most frequent wave state (184 occurrences) also happened in the same condition.

Figure 30. Combined scatter and energy diagrams of Leixoes in different ranges of H_s and T_e

According to Figure 31, the wave energy scatter diagram of Matosinhos indicates that the peak power and the most frequent one (156 occurrences) occurs for T_e between 8-10 s and H_s between 1-2 m. The peak energy at Matosinhos is slightly less than that of Leixoes and it is approximately 1.5 MWhr/m during the 25 days.

Figure 31. Combined scatter and energy diagrams of Matosinhos in different ranges of H_s and T_e

According to Figure 32, the wave energy scatter diagram of Aveiro indicates that the peak power occurs for T_e between 8-10 s and H_s between 1-2 m. However, the most frequent waves (161 occurences) occur for T_e between 6-8 s and H_s between 1-2 m. Also, Aveiro's peak energy is similar to that of Matosinhos and it is approximately 1.5 MWhr/m during the 25 days of computation.
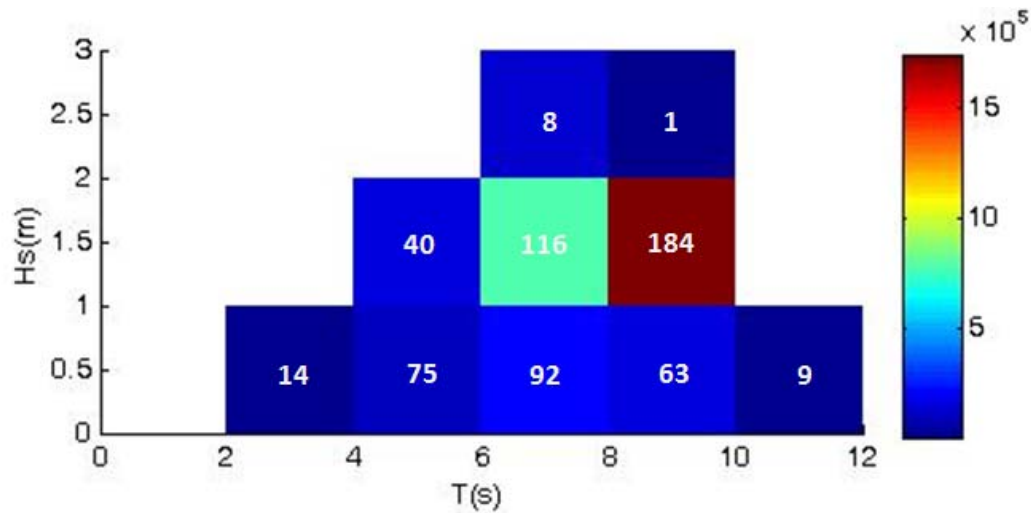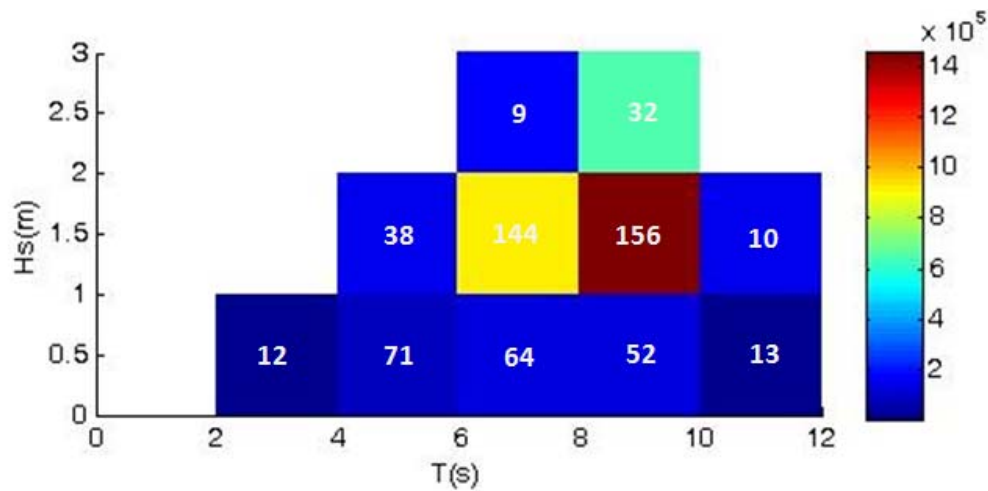
45
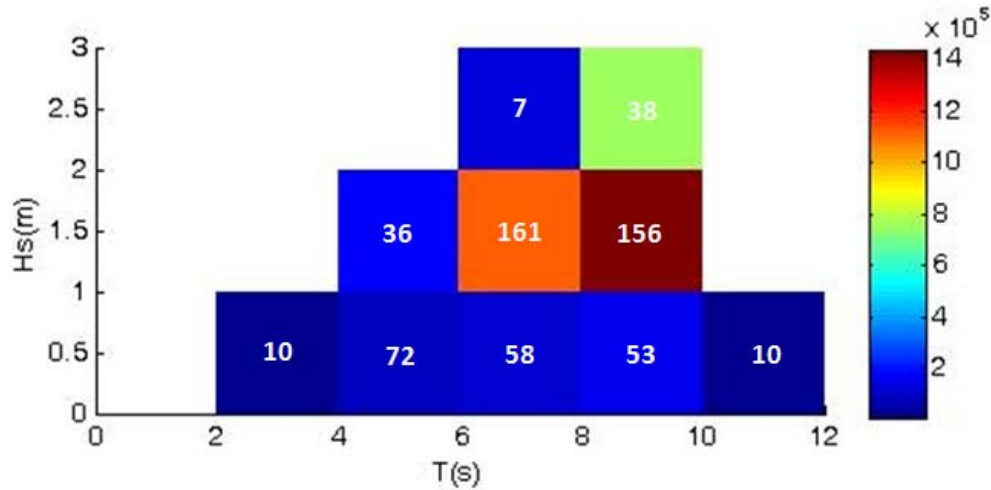
Figure 32. Combined scatter and energy diagrams of Aveiro in different ranges of H_s and T_e

According to figures 33-37, the wave energy scatter diagram of the southern part of the Portuguese western coast shows that the dominant T_e value is lower than that of the stations of the north model and ranges between 4-6 s. These lower T_e values in combination with H_s values produce less power than the higher T_e and H_s combinations of north model stations. The only exception to this rule is Figueira da Foz which has the highest peak power between the nine stations and it is approximately 2.6 MWhr/m during the computational period. This difference in wave power for each T_e and H_s combination accumulates and produces a lower wave energy scatter at the platform. This is the reason why the peak wave energy at the south model stations is between 1.2-1.5 MWhr/m even though the largest wave energy magnitude of the Cascais, Peniche and Sines is more than the wave energy magnitude (figures 11 and 12) of the north model stations. The possible reason for the lower T_e values and consequently lower scatter energy distribution at the locations of the south model may be due to their water depth and their longer distance from the shore (figures 17 and 18). This implies that unlike the north model exposed at approximately 180° due to their close proximity to the shore, the platform is exposed to multidirectional locally generated wind- and wave fields. Locally generated wave fields are short period waves still being created by winds.

Figure 33. Combined scatter and energy diagrams of Figueira da Foz in different ranges of H_s and T_e

Figure 34. Combined scatter and energy diagrams of Cascais in different ranges of H_s and T_e

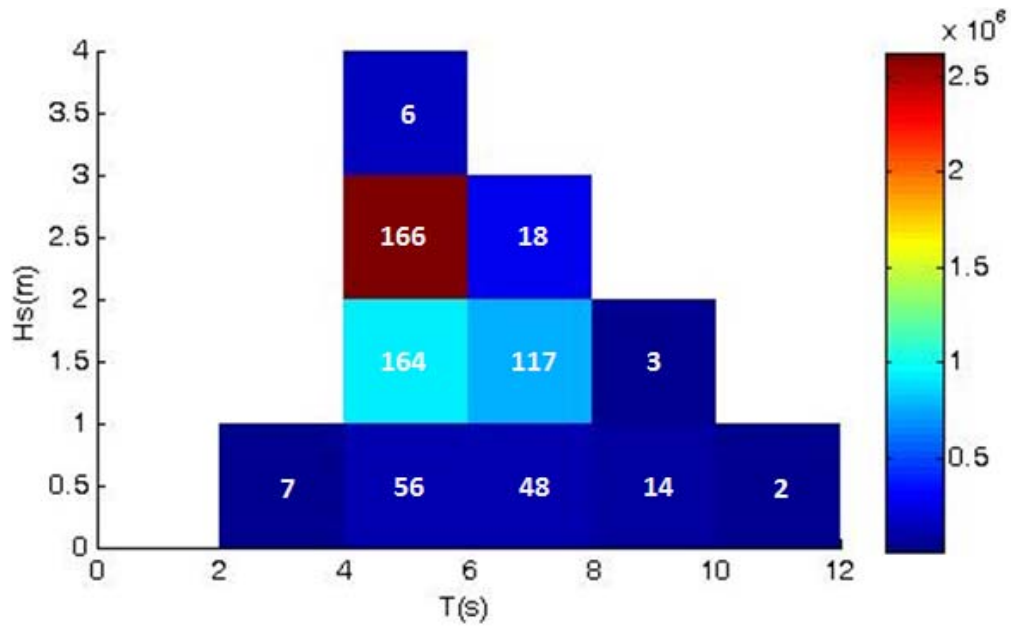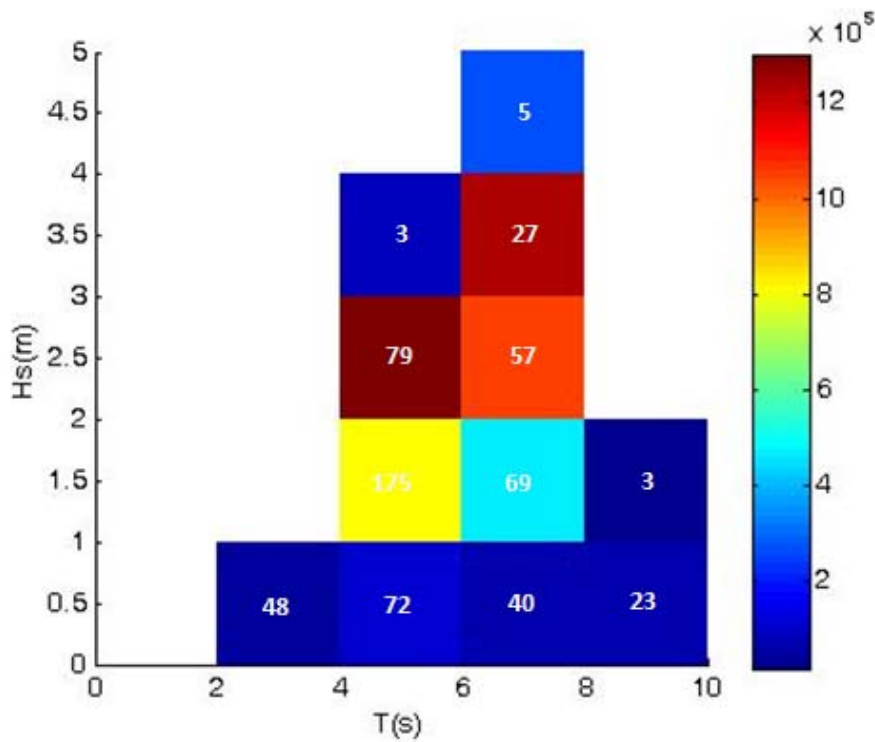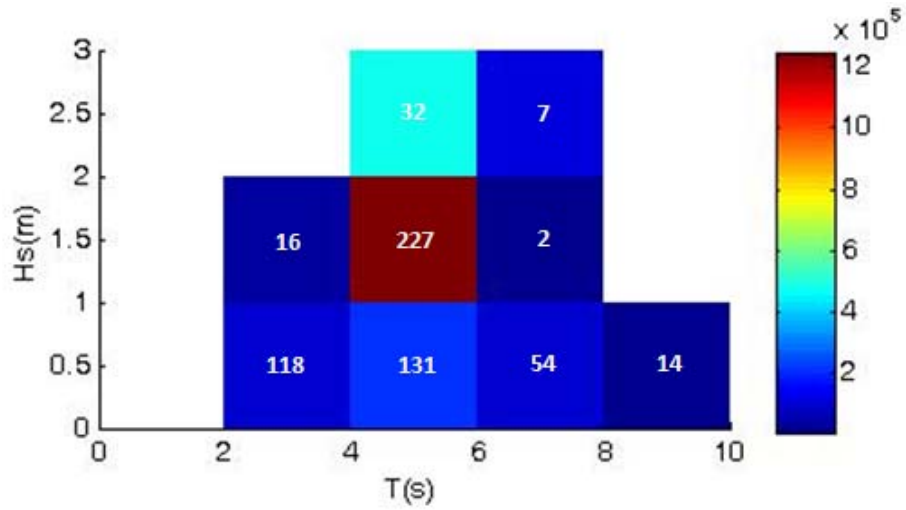**Figure 35. Combined scatter and energy diagrams of Sesimbra in different ranges of H_s and T_e**
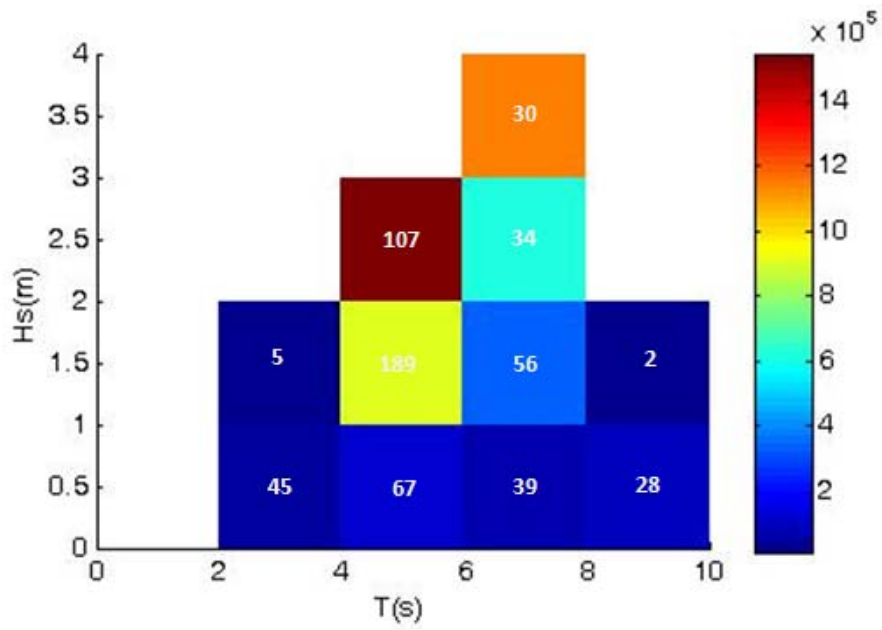
Figure 36. Combined scatter and energy diagrams of Peniche in different ranges of H_s and T_e
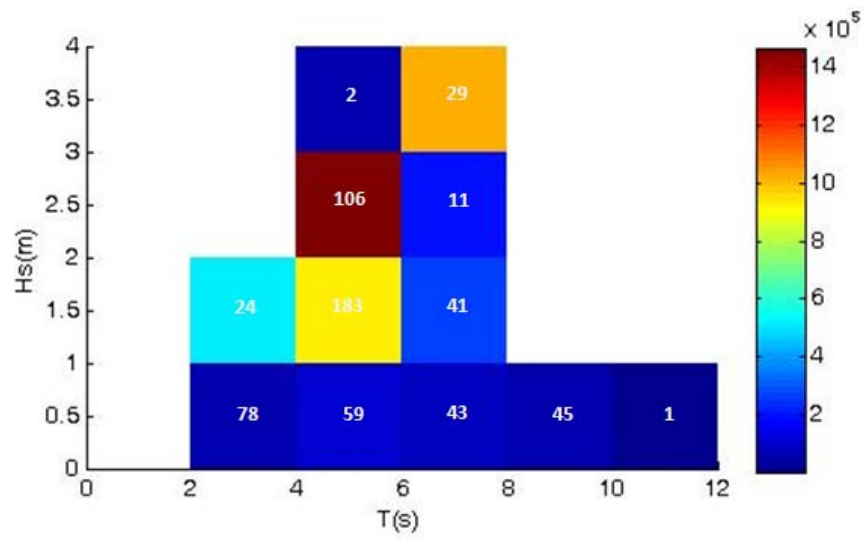
Figure 37. Combined scatter and energy diagrams of Sines in different ranges of H_s and T_e

6. Summary and Conclusion

The presented work focused on the numerical modeling of the energy resources of nearshore and offshore waves in the Portuguese western coast. In this thesis, a novel method was introduced and developed in order to calculate nearshore and offshore wave energy and to predict wave behavior as accurately as possible. Delft3D software package was used to simulate nearshore and offshore waves by taking flow hydrodynamics into account. The software used a third generation wave model, namely SWAN in order to simulate the wave parameters. Such energy prediction and calculation methods can be applied to different types of oscillating bodies.

According to section 3, the wave modeling is reliable since the modeled wave heights and periods agree with values observed at the measurement stations.

Based on the summary made and the conclusions drawn from the findings of this study, the resulting description of the Portuguese wave power obtained from the study area can serve as a representative indicator of wave power conditions. Input data were based on *Magicseaweed* online database which was available for every three hours. The results could be used to identify areas of wave power concentration in order to locate the suitable places for installing WEC units. It was shown that the model accurately estimates the offshore and nearshore wave power resources by considering time-varying boundary conditions. However, further numerical modeling is required for detailed design of wave farms especially for survivability analyses. Such analysis will also provide more accurate estimations of wave power conditions in shallow water locations (less than approximately 50m). Resource monitoring can ensure device survivability by enforcing generation cut off during extreme waves.

7. Recommendations for Future Works

This thesis has been a first step in determining the wave power magnitude of the Portuguese coast by considering Wave and Flow modules simultaneously, but there is still much work that can and should be done before wave energy projects can proceed. First and foremost, wave energy storage is an important issue, and further study is required to determine solutions which are both possible and economically viable.

Also, more studies need to find the exact effect of the wave on sediment transportation, water depth and flow modules and vice-versa which are not the main focus of this work. With these studies, sediment transportation can be predicted and can be prevented in places where they might cause some problems. For example, Delft3D online module (Wave-Flow) can be used in order to investigate sediment transportation in Figueira da Foz and many other places along the western coast of Portugal which has been causing some problems for those whose houses are located near the shore.

The economic analysis of the practical installation of WECs was not the focus of this thesis and since the investors are always seeking the economical outcome of projects, it is important to conduct a thorough and detailed investigation regarding the costs and sensitivities of the factors contributing to the overall economics of WEC installations and the electricity produced from wave energy.

The wave climate in the area, while specified somewhat in this thesis, could be used in detailed investigations of the behavior of shallow-water, as well as further study regarding the changes of wave climate over a number of years.

One final important factor which should not be overlooked but is beyond the scope of this thesis is energy policy. No wave energy policies are currently being outlined around the world, and it is up to engineers, policy makers, economists, and a variety of others from multiple disciplines to come together and find a way to make it happen.

References

[1] Saket A., Etemad-Shahidi A. *Wave energy potential along the northern coasts of the Gulf of Oman, Iran.* Renewable Energy, Vol. 40, pp. 90-97 (2012).

[2] Falcao, A.F. de O. *Wave energy utilization: A review of the technologies*, Renewable and Sustainable Energy Reviews, Vol.14, pp. 899 – 918, (2010).

[3] Ris R.C., Holthuijsen L.H., Booij N. *A third-generation wave model for coastal regions 2: verification.* J Geophys Res-Oceans, Vol. 104, pp. 7667-7681 (1999).

[4] Hirohisa T. *Sea trial of a heaving buoy wave power absorber.* In: Berge H, editor. *Proceedings of 2nd International Symposium on Wave Energy Utilization*, Trondheim, Norway, pp. 403–17 (1982).

[5] CRES (Centre for Renewable Energy Sources). *Ocean Energy Conversion in Europe – Recent advancements and prospects.* Published in the framework of the ''Coordinated Action on Ocean Energy'' EU project under FP6 Priority: 6.1.3.2.3; Renewable Energy Technologies with the support of the European Commission Directorate-General for Research under contract SES6-CT2004-502701 (2006).

[6] Cle´ment A., McCullen P., Falca˜o A., Fiorentino A., Gardner F., Hammarlund K., et al. *Wave energy in Europe: current status and perspectives.* Renewable and Sustainable Energy Reviews;Vol. 6, pp. 405–31 (2002).

[7] Aguiar R., Pontes M.T., Oliveira Pires H. *A Nearshore Wave Energy Atlas for Portugal.* Proc 22nd Int Conf on Offshore Mechanics and Arctic, pp. 37407 (2003).

[8] Guedes Soares C., Weisse R., Carretero J.C., Alvarez E. *A 40 years hindcast of wind, sea level and waves in European waters.* Proceedings of the 21st International Conference on Offshore Mechanics and Arctic Engineering (OMAE'02), ASME Paper OMAE2002–SR28604 (2002).

[9] Guedes Soares C. *Hindcast of dynamic processes of the ocean and coastal areas of Europe.* Coastal Engineering, Vol. 55, pp. 825–6 (2008.02.007).

[10] Pilar P., Guedes Soares C., Carreterro J.C. *44-year wave hindcast for the North East Atlantic European coast.* Coastal Engineering, Vol. 55, pp. 861–71 (2008).

[11] Rusu L., Pilar P., Guedes Soares C. *Hindcast of the wave conditions along the west Iberian coast.* Coastal Engineering Vol. 55, pp. 906–19 (2008).

[12] Falnes, J. *Review A review of Wave-Energy Extraction*, Marine Structures, pp. 185–201 (2007).

[13] Federal Energy Management Programme, FEMP, *Ocean Energy Technology Overview*, The U.S. Department of Energy, July DOE/GO-102009-2823 (2009).

[14] AEA, *Review and Analysis of Ocean Energy Systems Development and Supporting Policies*, IEA's, Implementing Agreement on Ocean Energy Systems, 28th June

(2006).

[15] Ringwood J. *Practical Challenges in Harvesting Wave Energy*, ECOR Symposium, St. John's, Newfoundland, October (2008).

[16] Electrical Power Research Institute, EPRI, *Ocean Tidal and Wave Energy*, Renewable Energy Technical Assessment Guide—TAG-RE (2005).

[17] Al-Habaibeh A., Su D. McCague, J., Knight, A., *An Innovative Approach For Energy Generation From Waves*, GCREEDER 2009, Amman-Jordan, March 31st – April 2nd (2009).

[18] GreenOceanEnergy ltd, *http://www.greenoceanenergy.com/*, Accessed on 20 July (2010).

[19] Waveberg, *http://www.waveberg.com*, Accessed on July (2010).

[20] Ross H. *Design, simulation, and testing of a novel hydraulic power take-off system for the Pelamis wave energy converter,* Renewable Energy pp. Vol. 31, pp. 271–283 (2006).

[21] Barker G., Vantorre M., Banasiak R., Beels C., and De Rouck J., *Numerical Modelling of Wave Energy Absorption By A Floating Point Absorber System*, Proceedings of the Seventeenth (2007) International Offshore and Polar Engineering Conference, Lisbon, Portugal, July 1-6 (2007).

[22] Falnes J., Lillebekken P.M. *Budal's Latching-Controlled-Buoy Type Wave-Power Plant*, 5th European Wave Energy Conference, Cork. Ireland 17th to 20th September (2003).

[23] Weinstein, A., Fredrikson G., Parks M.J., Nielsen K., *AquaBuOY, The Offshore Wave Energy Converter Numerical Modelling And Optimization*. Proceedings of MTTS/IEEE Techno-Ocean'04 Conference, Kobe, Japan; 2004, vol. 4, pp. 1854–59 (2004).

[24] Prado, M., (2008), "Archimedes Wave Swing (AWS)", *Cruz J, editor. Ocean Wave Energy. Berlin: Springer*; pp. 297–304 (2008).

[25] Gardner F.E., *Learning Experience of AWS Pilot Plant Test Offshore Portugal.* Proceedings of 6th European Wave Energy Conference; 2005. pp. 149–54 (2005).

[26] McCabe A. P., Bradshaw A., Meadowcroft J.A.C., Aggidis. G., *Developments In The Design Of The PS Frog Mk 5 Wave Energy Converter*. Renewable Energy, Volume 31, pp. 141–51 (2006).

[27] Babarit A., Clement A.H., Gilloteaux J.C., *Optimization and Time-Domain Simulation of the SEAREV Wave Energy Converter*. Proceedings of 24th International Conference Offshore Mechanics Arctic Engineering, Halkidiki, Greece; 2005, vol. 2, pp. 703–12., (2005).

[28] Davis R. and Hayes M.O., *What is a wave-dominated coast?,* Marine geology, 60(1-4): 313-329 (1984).

[29] Holthuijsen L.H., *Waves in Oceanic and Coastal Waters*, Cambridge University Press (2007).

[30] Sverdrup K., Duxbury A.C. and Duxbury A.B., *An Introduction to the World's Oceans*, McGraw-Hill Publishers (2004).

[31] Kim G., Jeong W.M., Lee K.S., Jun K., Lee M.E. *Offshore and Nearshore wave energy assessment around the Korean peninsula.* Energy, Vol. 36, pp. 1460-1469 (2011).

[32] Rafael W., Jens E., Jan I., Mats L. *Wave climate off the Swedish west coast.* Renewable Energy, Vol. 34, pp. 1600-1606 (2009).

[33] Longuet-Higgins M.S. and Stewart R.W., *Changes in the Form of Short Gravity Waves on Long Waves and Tidal Currents.* Deep-Sea Research (1960).

[34] Longuet-Higgins M.S., *Longshore Currents Generated by Obliquely Incident Sea Waves*, 1. Journal of Geophysical Research, Vol. 75, pp. 6778-6789 (1970).

[35] Longuet-Higgins M.S. and Stewart R.W., *Radiation stresses in water waves; a physical discussion, with applications.* Deep-Sea Research, Vol. 11, pp. 529-562 (1964).

[36] Treffers R. *Wave-Driven Longshore Currents in the Surf Zone*, Deltares (2008).

[37] Battjes J.A., *Modeling of turbulence in the surf zone.* In: Proc. Symp. Modeling Techniques, ASCE: pp. 1050-1061 (1975).

[38] Dally W.R. *Surf zone processes, Encyclopedia of Coastal Science.* Springer Netherlands, pp. 804-807 (2005).

[39] Davis R. and Hayes M.O. *What is a wave-dominated coast?* Marine geology, Vol. 60, pp. 313-329 (1984).

[40] Thomson R.E. *Oceanography of the British Columbia Coast* (1981).

[41] Henry A., Doherty K., Cameron L., Whittaker T., Doherty R., *Advances in the design of the Oyster wave energy converter.* In: Proc. Royal Institution of Naval Architect's, Marine and Offshore Renewable Energy Conference. London (2010).

[42] Fernandes A.M., Fonseca N. *Finite depth effects on the wave energy resource and the energy captured by a point absorber*, Ocean Engineering Vol. 67, pp. 13 – 26 (2013).

[43] Lesser G.R., Roelvink J.A., Kester J.A.T.M. and Stelling G.S., *Development and validation of a three-dimensional morphological model*, Coastal Engineering, Vol. 51, pp. 883-915 (2004).

[44] Deltares, Delft3D - Flow Manual, Deltares, Delft (2011).

[45] Booij N., Haagsma I.J.G., Holthuijsen L.H., Kieftenburg A.T.M.M., Ris R.C., van der Westhuysen A.J., Zijlema *"SWAN Cycle III version 40.41 User Manual"* Delft University, (2004).

[46] Coastal Engineering Manual (CEM), US Army Corp of Engineers (2002).

[47] Van Tonder A. *"A software package for the simulation of three-dimensional sea states in the laboratory"*, report on wave generation for physical modeling for the CSIR (1992).

Appendix:

Input data for boundary conditions:

Table 3. Boundary conditions for north orientation of north model (Figure 11)

Date (yyyymmdd)	Significant Wave Height	Wave Period	Wave Direction (°)
20130830	0.3	14	299
20130831	0.8	11	302
20130901	0.8	10	302
20130902	1.2	12	323
20130903	0.9	11	328
20130904	0.4	14	293
20130905	0.8	12	288
20130906	0.6	10	287
20130907	1.7	11	322
20130908	2.1	6	350
20130909	0.6	8	313
20130910	0.8	9	304
20130911	2.7	8	4
20130912	0.5	8	1
20130913	0.3	10	311
20130914	0.8	12	306
20130915	1.4	13	317
20130916	1.2	11	316
20130917	2.9	13	342
20130918	2.1	12	332
20130919	2.3	12	336
20130920	1.4	10	322
20130921	1.1	9	305
20130922	0.9	9	300
20130923	1.4	13	305
20130924	1.7	11	267

Table 4. Boundary conditions for south orientation of north model (Figure 11)

Date (yyyymmdd)	Significant Wave Height	Wave Period	Wave Direction (°)
20130830	0.3	11	319
20130831	0.6	11	298
20130901	0.8	10	302
20130902	0.6	9	303
20130903	0.9	11	318
20130904	0.5	10	322
20130905	0.8	11	288
20130906	0.8	10	287

20130907	2.1	8	320
20130908	2	8	323
20130909	1	8	327
20130910	0.6	8	308
20130911	1.5	8	321
20130912	0.3	9	292
20130913	0.2	10	310
20130914	0.6	13	301
20130915	0.8	11	306
20130916	1.8	8	319
20130917	1.5	7	321
20130918	1.2	12	318
20130919	1.7	7	328
20130920	1.2	11	317
20130921	1.5	9	319
20130922	1.1	9	312
20130923	0.8	13	304
20130924	1.1	11	282

Table 5. Boundary conditions for north orientation of south model (Figure 17)

Date (yyyymmdd)	Significant Wave Height	Wave Period	Wave Direction (°)
20130830	1.1	7	332
20130831	0.8	11	296
20130901	1.1	11	311
20130902	0.8	13	308
20130903	0.8	11	315
20130904	0.4	9	320
20130905	0.8	11	286
20130906	0.8	10	287
20130907	1.8	8	322
20130908	2	8	323
20130909	0.6	9	322
20130910	1.1	7	318
20130911	1.7	8	321
20130912	1.2	8	334
20130913	0.5	4	331
20130914	0.6	13	296
20130915	0.8	10	300
20130916	1.7	7	320
20130917	2	7	322
20130918	2.3	7	329
20130919	1.2	11	319
20130920	1.2	11	309
20130921	1.5	9	316

20130922	1.1	9	309
20130923	1.1	11	299
20130924	1.2	11	273

Table 6. Boundary conditions for south orientation of south model (Figure 17)

Date (yyyymmdd)	Significant Wave Height	Wave Period	Wave Direction (°)
20130830	0.6	8	316
20130831	0.5	12	304
20130901	0.6	9	315
20130902	0.6	10	310
20130903	0.9	11	321
20130904	0.4	10	323
20130905	0.6	12	295
20130906	0.6	10	294
20130907	1.2	9	313
20130908	1.4	10	320
20130909	1.2	7	324
20130910	1.1	6	321
20130911	0.9	7	316
20130912	0.9	9	323
20130913	0.5	8	323
20130914	0.4	11	316
20130915	0.9	8	319
20130916	1.1	12	318
20130917	1.2	8	316
20130918	1.4	9	319
20130919	1.5	8	323
20130920	0.9	8	316
20130921	1.1	10	319
20130922	0.8	9	312
20130923	0.9	14	315
20130924	0.5	12	289